Downloaded from genome.cshlp.org on November 29, 2026 . Published by Cold Spring Harbor Laboratory Press



Engineering genome instability at repetitive elements reveals distinct roles for balanced rearrangements and ploidy in adaptation of a human fungal pathogen

Matt Shaw, Samuel Vega-Estevez, Robert Jordan Price, et al.

Genome Res. published online November 24, 2026
Access the most recent version at doi:10.1101/gr.281873.126

P<P Published online November 24, 2026 in advance of the print journal.

Accepted Manuscript Peer-reviewed and accepted for publication but not copyedited or typeset; accepted manuscript is likely to differ from the final, published version.

Open Access Freely available online through the *Genome Research* Open Access option.

Creative Commons License This manuscript is Open Access.This article, published in *Genome Research*, is available under a Creative Commons License (Attribution 4.0 International license), as described at http://creativecommons.org/licenses/by/4.0/.

Email Alerting Service Receive free email alerts when new articles cite this article - sign up in the box at the top right corner of the article or **click here.**



To subscribe to *Genome Research* go to:
https://genome.cshlp.org/subscriptions

Published by Cold Spring Harbor Laboratory Press

Downloaded from genome.cshlp.org on November 29, 2026 . Published by Cold Spring Harbor Laboratory Press

Engineering genome instability at repetitive elements reveals distinct roles for balanced rearrangements and ploidy in adaptation of a human fungal pathogen

Matthew Shaw[1], Samuel Vega-Estevez[1], R. Jordan Price[2], Jack Davis[1], Chloe Uyl[1, #a] and Alessia Buscaino[1; #a; #b; #c *]

[1] Kent Fungal Group, School of Natural Sciences, University of Kent, Canterbury, CT2 7NZ, United Kingdom

[2] NIAB, Park Farm, Villa Road, Histon, Cambridge, CB24 9NZ, United Kingdom

[#a] Current address: Quadram Institute Bioscience, Norwich Research Park, Norwich, NR4 7UQ, United Kingdom

[#b] Current address: Centre for Microbial Interactions, Norwich Research Park, Norwich, NR4 7UG, United Kingdom

[#c] Current address: University of East Anglia, Norwich, NR4 7TJ, United Kingdom

*Corresponding author

Email: Alessia.Buscaino@quadram.ac.uk

Running title: Balanced rearrangements in *Candida albicans*

Downloaded from genome.cshlp.org on November 29, 2026 . Published by Cold Spring Harbor Laboratory Press

ABSTRACT

Genome plasticity is a ubiquitous feature of eukaryotic life, yet how different forms of genome variation contribute to biological adaptation remains poorly understood. Fungal pathogens exploit genome instability for adapting rapidly to stress. In the human fungal pathogen *Candida albicans*, structural variation frequently arises at repetitive DNA elements and generates balanced chromosomal rearrangements, loss of heterozygosity and aneuploidy. Because these genome alterations often coexist in clinical isolates, their individual contributions to adaptation remain difficult to resolve.

Here, we describe Repetitive Element–Directed Cas9 (RED-Cas9), a genome engineering approach that introduces targeted double-strand breaks at two major *C. albicans* repeat families. By generating multiple classes of structural variation within the same genetic background, RED-Cas9 enables the direct comparison of their biological consequences, avoiding the confounding effects of unrelated genetic variation present in clinical isolates. We show that balanced rearrangements, which rearrange chromosomes without altering gene dosage, produced minimal transcriptional changes and no large-effect phenotypes. In contrast, ploidy variation triggered widespread gene dosage–linked transcriptional reprogramming and distinct phenotypic outcomes, including fluconazole resistance, impaired filamentation, and reduced virulence.

These findings establish RED-Cas9 as a platform to dissect the functional consequences of distinct classes of structural variation and demonstrate that balanced chromosomal rearrangements and chromosome copy-number changes make fundamentally different contributions to genome plasticity and adaptation in a human fungal pathogen.

INTRODUCTION

Pathogens must continually adapt to survive in the changing environments posed by immune defences and antifungal drugs (Hitzler et al. 2025). A central strategy for this adaptation is genome plasticity, which generates genetic diversity on which selection can act. In fungi, genome plasticity underpins phenotypic flexibility, enabling rapid shifts between

Downloaded from genome.cshlp.org on November 29, 2026 . Published by Cold Spring Harbor Laboratory Press

commensal and pathogenic states, tolerance to stress, and resistance to antifungal drugs (Beekman and Ene 2020). Among fungal pathogens, *Candida albicans* stands out as a model for understanding how genomic variation fuels adaptive potential. *C. albicans* is a diploid yeast that normally colonizes the human gastrointestinal and urogenital tracts as a commensal but can cause life-threatening systemic infections (Schille et al. 2025; Denning 2024). Clinical isolates of *C. albicans* are highly heterogeneous, differing in stress tolerance, host colonization efficiency, and virulence (Hirakawa et al. 2015; Anderson et al. 2023; Ropars et al. 2018; Cravener et al. 2023; Iracane et al. 2024). This phenotypic diversity is often associated with extensive genomic diversity, including single nucleotide polymorphisms (SNPs), insertions and deletion (indel) mutations, loss of heterozygosity (LOH) and extensive chromosomal variation (Selmecki et al. 2006; Todd and Selmecki 2020; Selmecki et al. 2010; Ene et al. 2019; Dunn and Anderson 2019; Ford et al. 2015). Environmental stresses, including host microenvironments and antifungal exposure, exacerbate this variability and select for adaptive rearrangements (Forche et al. 2009, 2011; Freire-Benéitez et al. 2016a; Ene et al. 2018).

Structural genomic variation can be broadly categorized into balanced and unbalanced chromosomal changes (Sreenivasan et al. 2025; Spielmann et al. 2018). Balanced structural variants (SVs), including inversions and reciprocal translocations, preserve gene dosage but reorganize genome architecture. These changes can alter transcription by relocating genes into different chromatin environments or by altering long-range regulatory interactions (Harewood et al. 2010; Sun et al. 2024; Lupiáñez et al. 2015). In contrast, unbalanced SVs, such as segmental duplications or aneuploidies, alter gene dosage and consequently gene expression (Beach et al. 2017; Ben-David and Amon 2020; Hou et al. 2018). In clinical populations of *C. albicans*, both balanced and unbalanced variants occur frequently (Hirakawa et al. 2015; Ropars et al. 2018; Ford et al. 2015; Scott et al. 2026). The consequences of chromosome copy-number changes are relatively well understood: *C. albicans* exhibits little transcript-level dosage compensation, such that chromosome copy-number changes generally produce proportional changes in gene expression. While some

Downloaded from genome.cshlp.org on November 29, 2026 . Published by Cold Spring Harbor Laboratory Press

buffering occurs at the proteome level, dosage imbalance drives substantial phenotypic change and adaptation under selective pressure (Mackey et al. 2025; Muenzner et al. 2024). Consistent with these effects, whole chromosome aneuploidies are associated with antifungal tolerance and resistance (Anderson et al. 2017; Hirakawa et al. 2017; Sun et al. 2023; Todd and Selmecki 2020; Yang et al. 2013, 2017, 2019, 2023).

LOH is an intermediate variant type, which maintains gene dosage but alters the relative haplotype balance. These too are common in clinical isolates (Ropars et al. 2018; Scott et al. 2026), and contribute to adaptation by unmasking recessive alleles, fixing beneficial mutations, and altering allele-specific gene expression and function (Ciudad et al. 2016; Forche et al. 2011; Ford et al. 2015).

In contrast, the consequences of balanced chromosomal rearrangements remain poorly understood. Nevertheless, work in diverse systems has shown that balanced rearrangements, such as inversions and translocations, can profoundly influence gene regulation by reorganizing chromosome architecture, altering chromatin context, modifying long-range regulatory interactions, and reshaping three-dimensional genome organization (Lupiáñez et al. 2015; Harewood et al. 2010; Sun et al. 2024). Balanced rearrangements occur frequently in *C. albicans* (Oggenfuss et al. 2025; Iwaguchi et al. 2001; Thrash-Bingham and Gorman 1992; Todd et al. 2019), yet whether they contribute to adaptation and phenotypic diversification through similar mechanisms remains largely unknown. Progress has been hindered partly by the extensive genetic heterogeneity of natural isolates, in which SNPs, indels, LOH events, and multiple chromosomal rearrangements coexist and obscure the individual effects of specific structural variants.

CRISPR-Cas9-mediated targeting of repetitive genomic elements has emerged as a strategy to generate chromosomal rearrangements circumventing the heterogeneity inherent to natural isolates (Fleiss et al. 2019; Yadav et al. 2020; Qi et al. 2023; Liu et al. 2022). However, no study to date has used this strategy to directly compare the relative contributions of balanced and unbalanced rearrangements within a single system, and this approach has not previously been applied to *C. albicans*, a fungal pathogen in which this

Downloaded from genome.cshlp.org on November 29, 2026 . Published by Cold Spring Harbor Laboratory Press

exact spectrum of rearrangement classes is already known to occur in clinical isolates (Ene et al. 2019; Anderson and Dietz 2024; Rustchenko 2007; Dunn and Anderson 2019; Selmecki et al. 2010).

Large-scale genome changes in *C. albicans* often occur at repeat-rich regions (Todd et al. 2019; Dunn and Anderson 2019). Two families of repeats are frequently associated with chromosome breakpoints: Major Repeat Sequences (MRS) and *TLO*-associated Recombination Elements (TRE). MRS elements are large (10–100 kb) arrays found proximal on seven of the eight chromosomes, composed of tandem 2.1 kb RPS units flanked by HOK and RB2 elements (Fig. 1B) (Magee et al. 1987; Chibana and Magee 2009; Dunn and Anderson 2019; Chu et al. 1993). The significance of these elements on *C. albicans* evolution is unclear but it has been shown that MRS size affects chromosome segregation fidelity (Lephart et al. 2005; Lephart and Magee 2006). MRS size and copy-number vary between strains and even between homologous chromosomes within a single strain (Asakura et al. 1991; Iwaguchi et al. 1992; Magee 1993). MRS-mediated reciprocal translocations have been independently mapped in multiple, unrelated clinical isolates (Chu et al. 1993; Butler et al. 2009; Chibana et al. 2000). Genomic changes at MRS loci also arise in direct response to host immune challenge (Smith et al. 2022) or during passage through a murine gastrointestinal model (Ene et al. 2018).

TRE elements (~200 bp) are recombination-prone fragile sites located at the 3′ end of *TLO* genes, which encode components of the Mediator transcriptional regulatory complex (Freire-Benéitez et al. 2016b; Haran et al. 2014; Dunn and Anderson 2019). Full-length or partial TREs are positioned immediately downstream of most *TLO* Open Reading Frames (ORFs) at subtelomeric regions, and a partial TRE element is also found downstream of *TLO34*, the only *TLO* gene located in a non-subtelomeric region, on Chr1 (Fig. 1B) (Freire-Benéitez et al. 2016b; Dunn and Anderson 2019). Beyond the marked expansion of the *TLO* family relative to closely related species, TRE-mediated subtelomeric recombination is an active, ongoing process as demonstrated by evolution experiments (Anderson et al. 2015).

Sequencing of *TLO*/TRE architecture across 23 genetically diverse clinical strains likewise

Downloaded from genome.cshlp.org on November 29, 2026 . Published by Cold Spring Harbor Laboratory Press

revealed extensive intra-species structural diversity at these loci (Dunn et al. 2022; Hirakawa et al. 2015). This recombination-prone architecture is associated with virulence-related *TLO* copy-number variation among isolates (Jackson et al. 2009; Haran et al. 2014; Flanagan et al. 2018; Fletcher et al. 2023).

To disentangle the effects of balanced and unbalanced chromosomal variation on *C. albicans* biology, we developed the RED-Cas9 system to introduce double-strand breaks at MRS and TRE repeats. By targeting these SV-associated repetitive elements, we reproduce variants as seen in clinical isolates. This produced a panel of structural variant genomes, spanning simple balanced rearrangements to complex rearrangements accompanied by aneuploidy and LOH in an otherwise isogenic background. This approach allows us to assess the relative effects of distinct structural variant classes on gene expression, fitness, and phenotypic variability.

RESULTS

Inducing DNA breaks at *C. albicans* repeats using RED-Cas9

To examine the impact of structural variation on *C. albicans* biology independently of additional confounding variants, we developed the RED-Cas9 system. In this system, single guide RNAs (sgRNAs) direct CRISPR-Cas9 to introduce double-strand breaks (DSBs) within MRS (RB2 and RPS) and TRE elements (Fig. 1A and Fig. 1B). As no exogenous repair template is supplied, these targeted DSBs mimic endogenous DNA damage. We hypothesized that breaks at these loci would be repaired using allelic or non-allelic repeat copies as templates, leading to structural rearrangements (Fig. 1A). In the RED-Cas9 system, *CAS9* is integrated at the *HIS1* locus and can be excised using a maltose-inducible FLP recombinase, allowing the system to be recycled (Nguyen et al. 2017).

Karyotypic analysis by contour-clamped homogeneous electric field (CHEF) gel electrophoresis showed that RED-Cas9 targeting of either MRS or TRE sites frequently produces gross chromosomal alterations (12.7% of colonies screened; Fig. 1C; Supplemental_Table_S1). Representative transformants were subsequently characterized by long-read sequencing (discussed later). Strains expressing RED-Cas9 with MRS- or

Downloaded from genome.cshlp.org on November 29, 2026 . Published by Cold Spring Harbor Laboratory Press

TRE-specific sgRNAs (MRS-g; TRE-g) displayed altered karyotypes compared to the parental SC5314 strain (Fig. 1C). To determine whether RED-Cas9 functions similarly in genetically distinct backgrounds**,** we repeated the experiment in the clinical isolate WO-1. This strain is karyotypically distinct from SC5314 and, unlike SC5314, retains an active RNA interference (RNAi) pathway (Iracane et al. 2024). Despite these differences, RED-Cas9 generated diverse karyotypes in this strain (Fig. 1D), demonstrating that repeat-directed DNA cleavage induces genome instability across genetically distinct *C. albicans* backgrounds. In contrast, control strains expressing Cas9 without sgRNAs (NG strains) showed no detectable changes (Fig. 1E).

To assess potential off-target effects of Cas9, we sequenced the genomes of RED-Cas9 strains (MRS-g1, -g2 and -g3; TRE-g1, -g3, -g4, -g5, -g7*;* mean depth >100x) using short-read Illumina technology and called variants (Supplemental_Table_S2; Supplemental_Table_S3.xlsx). Possible off-target sites were predicted, allowing up to five mismatches and one DNA and RNA bulge per guide RNA, limited to canonical NGG PAMs. Comparison of these predicted sites with genomic variants revealed no enrichment of small variants within off-target sites (Supplemental_Table_S4).

Together, these results show that RED-Cas9-induced DNA damage at repetitive elements drives large-scale genome rearrangements in *C. albicans*. These structural changes occur without detectable off-target effects, establishing RED-Cas9 as a robust system to dissect repeat-driven genome instability and its consequences for pathogen evolution.

RED-Cas9 induces repeat-driven structural variants

To define the spectrum of structural variants generated by RED-Cas9 and establish the genomic architecture of the resulting strains, we performed Oxford Nanopore Technologies (ONT) long-read genome sequencing on RED strains targeting MRS (MRS-g1, MRS-g2, MRS-g3) and TRE (TRE-g1 to TRE-g7) loci. Long-read sequencing (read depth: 47-109x; Supplemental_Table_S5) resolved the genomic architecture of the rearranged strains and enabled mapping of allelic transitions and structural variants that cannot be captured by

Downloaded from genome.cshlp.org on November 29, 2026 . Published by Cold Spring Harbor Laboratory Press

short-read sequencing. Analyses included both assembly-dependent and assembly-independent methods to fully characterize heterozygous structural variants. *De novo* haploid assemblies were highly complete (BUSCO completeness 97.6-98.4%; Supplemental_Table_S6). Assemblies were mapped to SC5314 A22 for initial karyotype screening (Supplemental_Fig_S1). As haploid assembly cannot fully capture structural heterozygosity, we performed structural variant calling to identify interchromosomal breakpoints, all of which occurred at target sites. We also identified breakpoint reads which spanned target sites and extended into different chromosomes, allowing us to characterize translocations (Supplemental_Table_S7). ONT data was further used to assess genome-wide allelic balance (Supplemental_Fig_S2) and coverage (Supplemental_Fig_S3), which were supported by Illumina data (Supplemental_Fig_S4).

Through these analyses, we identified three classes of chromosomal alteration associated with breakpoints at MRS or TRE elements: balanced rearrangements, extended LOH tracts, and unbalanced copy-number changes (Fig. 2). Interchromosomal rearrangements were detected in 9 of the 10 ONT-sequenced RED-Cas9 strains. For subsequent analyses, strains carrying rearrangements without detectable LOH or CNV were classified as balanced (3/10); strains that also carried extended LOH were classified as LOH (3/10); and strains with unbalanced rearrangements were classified as CNV (4/10) (Fig. 2A; Supplemental_Table_S7).

The balanced group included strains with relatively simple translocations between two chromosomes (e.g. TRE-g1) and strains with complex balanced rearrangements involving several chromosomes (e.g. MRS-g1) (Fig. 2A; Supplemental_Table_S7). Strains in the LOH group carried either extended LOH tracts with breakpoints mapping to MRS or TRE elements (e.g. MRS-g3) or whole-chromosome LOH (Fig. 2B-C). Finally, the CNV group contained strains with unbalanced chromosomal alterations, including TRE-g6, which carried rearrangements involving Chr1, Chr2 and Chr3 and three copies of a partial Chr1 truncated at the *TLO34* Cas9 target site (Fig. 2D,E).

Downloaded from genome.cshlp.org on November 29, 2026 . Published by Cold Spring Harbor Laboratory Press

MRS length in RED-Cas9 edited strains was stable, with the only significant changes occurring in MRS-g1 and MRS-g3 (Supplemental_Table_S8). Targeting TRE elements frequently generated telomere-swapping events, although their exact frequency could not be determined because telomeric and subtelomeric sequences downstream of TRE loci are short and highly similar, limiting resolution even with long-read sequencing (Chibana et al. 1998; Hirakawa et al. 2015; Hoyer et al. 2024).

In every case, breakpoints localized to repeats and junctions joined one repeat copy to another, generating either long LOH tracts or chimeric chromosomes. This architecture is the signature of homologous recombination (HR) using an MRS or TRE copy as repair template, rather than non-homologous end joining (NHEJ), which religates broken ends locally without transferring flanking sequence, and often introduces breakpoint indels (Ran et al. 2013). To test this model, we focused on the non-subtelomeric *TLO34/*TRE34 locus. Rearrangements involving this locus were identified in all TRE strains. In each strain, the acentric Chr1 fragment fused with a subtelomeric *TLO/*TRE locus to form a fusion chromosome, while the remaining centromere-containing Chr1 fragment was truncated and stabilized by telomere addition. Telomeric repeats were identified at the breakpoint in nine of the ten characterized truncation events (Supplemental_Table_S7). Analysis of breakpoint-spanning reads showed that the *TLO*–TRE structure was reconstituted in almost all resolved rearrangements (18/22; Supplemental_Table_S7). Local assembly showed that the TRE34 sgRNA target was altered in every derivative examined. However, no derivative contained an indel absent from the parental TRE repertoire, and nearly all altered alleles (19/21) matched another TRE copy in parental SC5314 (Supplemental_Table_S9). This transfer of donor-associated polymorphisms, together with reconstitution of the *TLO*-TRE structure and the absence of novel indels, supports homologous recombination-mediated repair rather than untemplated NHEJ.

Together, these results demonstrate that RED-Cas9 is a useful genome editing tool for generating both balanced and unbalanced chromosomal rearrangements in *C. albicans*.

Downloaded from genome.cshlp.org on November 29, 2026 . Published by Cold Spring Harbor Laboratory Press

RED-Cas9 triggers frequent whole-chromosome ploidy changes

ONT coverage analysis of RED-Cas9 strains suggested the presence of chromosome copy-number changes. We therefore investigated whether repeat-directed DNA cleavage altered whole-genome or whole-chromosome ploidy. We first examined whole-genome ploidy by staining DNA with propidium iodide and analyzing the samples by flow cytometry. MRS-g2 exhibited a shift associated with an approximately tetraploid genome, whereas all other strains retained diploid DNA content (Fig. 3A and Supplemental_Fig_S5). Microscopy of MRS-g2 cells revealed phenotypes consistent with chromosome missegregation, including growth in a pseudo-hyphal form and an increased proportion of cells exhibiting abnormal nuclear numbers (Fig. 3B, Supplemental_Fig_S6).

To detect chromosomal aneuploidies, we analyzed read-depth profiles from ONT sequencing. Three of ten independently derived RED-Cas9 strains (30%) carried whole-chromosome copy-number alterations (Fig. 3C and 3E and Supplemental_Fig_S3), substantially exceeding the spontaneous frequency of whole-chromosome ploidy changes reported under standard laboratory conditions (Avramovska and Hickman 2019; Forche et al. 2011). Specifically, the tetraploid MRS-g2 strain contained three copies of both Chr4 and ChrR (Fig. 3C and 3E). TRE-g2 carried three copies of Chr5, and TRE-g7 three copies of both Chr4 and ChrR (Fig. 3D and 3E). Read-depth analysis of Illumina sequencing data and quantitative PCR validation support these findings (Supplemental_Fig_S4).

To determine whether these events resulted from Cas9 expression or transformation rather than repeat-directed DNA cleavage, we analyzed ten independent transformants carrying the Cas9 cassette integrated without an sgRNA (no-guide, NG). We used ONT sequencing to detect balanced and unbalanced chromosomal variations, and flow cytometry with propidium iodide (PI) staining to detect whole-genome ploidy changes. In contrast to RED-Cas9 strains, none of the NG strains showed chromosomal rearrangements or copy-number changes, and all were diploid (Supplemental_Fig_S7; Supplemental_Fig_S8; Supplemental_Fig_S9; Supplemental_Table_S7). This demonstrates that translocations and

Downloaded from genome.cshlp.org on November 29, 2026 . Published by Cold Spring Harbor Laboratory Press

whole-chromosome ploidy alterations are caused by repeat-directed DNA cleavage rather than Cas9 expression or transformation alone. We then tested whether balanced chromosome rearrangements generate genomes that are intrinsically unstable, leading to chromosome copy-number changes. To test this, we selected two strains carrying balanced rearrangements and no LOH (MRS-g1 and TRE-g5) and serially passaged nine single colonies per strain for approximately 250 generations. CHEF analysis detected no additional chromosome rearrangements following evolution (Fig. 3F). Independently, to determine whether balanced rearrangements increase the rate of genome instability, we introduced a heterozygous *URA3*$^{+}$ marker into the parental strain and MRS-g1, MRS-g3, TRE-g4, TRE-g5, TRE-g7 rearranged strains and quantified the frequency of *URA3*$^{+}$ loss by fluctuation analysis. No significant increase in *URA3*$^{+}$ loss frequency was detected relative to the parental strain (Supplemental_Fig_S10), further confirming that balanced rearrangements do not increase genome instability.

Together, these results demonstrate that repeat-directed DNA cleavage at repetitive elements induces whole-chromosome copy-number changes in *C. albicans*. The absence of chromosome copy-number alterations in NG controls confirms that these events are driven by targeted DNA cleavage, while the stability of balanced rearrangements indicates that they do not predispose cells to subsequent genome instability.

Balanced chromosomal rearrangements have minimal effects on gene expression

The diverse collection of RED-Cas9 strains provided an opportunity to examine how different classes of structural variation influence gene expression in *C. albicans*. Although transcriptional consequences of chromosome copy-number changes and LOH are relatively well characterized (Muzzey et al. 2014; Mackey et al. 2025; Liang et al. 2019), much less is known about the impact of balanced chromosomal rearrangements. We therefore focused our transcriptomic analysis on strains carrying balanced rearrangements while comparing them with strains carrying LOH or chromosome copy-number variation. To this end, we selected eight representative strains for transcriptome profiling by RNA-seq: three with

Downloaded from genome.cshlp.org on November 29, 2026 . Published by Cold Spring Harbor Laboratory Press

299 balanced rearrangements and no copy-number variation (MRS-g1, TRE-g1 and TRE-g5),
300 three with an extended tract of loss of heterozygosity (LOH; MRS-g3, TRE-g3, TRE-g4), and
301 two with extensive copy-number variation (MRS-g2 *and* TRE-g7). This analysis
302 demonstrated that balanced chromosomal rearrangements had negligible impact on global
303 gene expression (Fig. 4A). The number of significantly differentially expressed genes (DEGs;
304 *P*adj < 0.05, $|\log_2$ fold change$| \geq 0.5$) was very low (MRS-g1 = 4; TRE-g1 = 8 and TRE-g5 =
305 29) (Supplemental_Table_S10.xlsx). These findings indicate that extensive chromosome
306 reshuffling can occur with minimal disruption to the *C. albicans* transcriptome**.**
307 Because balanced rearrangements are expected to reposition genes into new chromatin or
308 nuclear environments, we examined the expression of genes located within ±10 kb of
309 rearrangement breakpoints. Excluding Cas9-targeted *TLO* genes, few of the nearby genes
310 showed significant expression changes (MRS-g1: 0/45; TRE-g1: 1/25; TRE-g5: 3/53) (Fig.
311 4B). Analysis of differential expression at breakpoints across balanced and LOH
312 (Supplemental_Fig_S11) strains revealed they were moderately enriched at *TLO34*
313 (Cochran–Mantel–Haenszel, BH corrected; 4/40; 10%, *P*adj = 0.0005), but not MRS element
314 (0/61; 0%, *P*adj = 1.00) or subtelomeric *TLO* (1/92; 1.1%, *P*adj = 0.62) breakpoints. Thus,
315 rearrangement at these loci can affect local gene expression but this is only significant when
316 the SV alters the local chromosome context, such as a neo telomere at *TLO34*. This result is
317 weaker than balanced structural variants in other eukaryotes which frequently alter
318 expression of genes by changing the local 3D genomic environment (Harewood et al. 2010;
319 Sun et al. 2024; Lupiáñez et al. 2015). This suggests balanced rearrangements between
320 these repeats are buffered, likely by shared chromosomal context, and chromatin state.
321 In contrast to balanced rearrangements, extended LOH tracts had a greater transcriptional
322 impact. Strain MRS-g3 displayed 132 DEGs, TRE-g3 displayed 14 and TRE-g4 displayed
323 103 (Fig. 4C, Supplemental_Table_S10.xlsx). Because LOH is known to unmask allelic
324 differences and modify gene expression (Liang et al. 2019; Ropars et al. 2018; Liang and
325 Bennett 2019), this mechanism likely underlies the observed changes. In LOH strains, DEGs
326 were enriched within LOH tracts and LOH chromosomes. In MRS-g3, DEGs were

Downloaded from genome.cshlp.org on November 29, 2026 . Published by Cold Spring Harbor Laboratory Press

significantly enriched at the ChrR LOH tract (33/703 expressed genes, 4.7% vs 1.7% background; Fisher's exact test, BH-corrected: OR = 2.79, *P*adj = 1.30×10^{-5}), but not the Chr5 LOH tract (7/220, 3.2%; OR = 1.86, *P*adj = 0.12). In TRE-g4, DEGs were enriched within the Chr1 LOH tract (23/582 expressed genes, 4.0% vs 1.4%; OR = 2.83, *P*adj = 1.30×10^{-4}). DEGs were also enriched on Chr6 (whole chromosome LOH) in TRE-g3 (10/440 expressed genes, 2.3% vs 0.07%; OR = 33.2, *P*adj = 2.37×10^{-9}).

Strains with altered ploidy (MRS-g2 and TRE-g7) exhibited the strongest transcriptional responses (Fig. 4D). Because MRS-g2 is tetraploid, we expect an overall increase in total mRNA output relative to the diploid parent (Yahya et al. 2022). However, this global increase is largely masked by standard RNA-seq normalization, which equalizes library sizes and thereby obscures changes in total transcript abundance (Evans et al. 2017; Li et al. 2017). Even so, copy-number effects remain evident: in MRS-g2, 581 DEGs were identified (Fig. 4D, Supplemental_Table_S10.xlsx). These show clear dosage-linked expression, with downregulated genes enriched on trisomic chromosomes (Supplemental_Fig_S12): Chr4 (97/673 expressed genes, 14.4%; Fisher's exact test: OR = 3.42, *P*adj = 4.16×10^{-1}□) and ChrR (128/987 expressed genes, 13.0%; OR = 3.26, *P*adj = 1.40×10^{-21}).

In TRE-g7, we identified 781 DEGs, of which upregulated genes were strongly enriched on trisomic chromosomes: Chr4 (285/671 expressed genes, 42.5%; Fisher's exact test: OR = 8.66, *P*adj = 6.73×10^{-1}□□) and ChrR (316/985 expressed genes, 32.1%; OR = 5.64, *P*adj = $1.71\times10^{-}$□³) (Fig. 4D; Supplemental_Fig_S12, Supplemental_Table_S10.xlsx). This is consistent with the dosage-dependent transcriptional effects previously reported in *C. albicans* aneuploid strains (Mackey et al. 2025; Yang et al. 2021). When grouped by genome type, CNV strains had significantly more DEGs than balanced strains (one-way ANOVA on $\log_{10}$ counts, *P* = 0.016; Tukey HSD, *P*adj = 0.013), with LOH strains intermediate. The CNV–LOH and LOH–balanced differences did not reach significance (*P*adj = 0.095 and 0.17). In all strains, DEGs were only significantly enriched on chromosomes which were aneuploid or had extended LOH tracts.

Downloaded from genome.cshlp.org on November 29, 2026 . Published by Cold Spring Harbor Laboratory Press

Together, these results demonstrate that different classes of structural variation have different consequences for gene expression in *C. albicans*. Balanced chromosomal rearrangements generated at MRS and TRE loci have minimal effects on both global and local transcription, whereas LOH produces intermediate transcriptional changes and chromosome copy-number variations generate extensive dosage-dependent transcriptional responses.

Balanced rearrangements show minimal fitness consequences, whereas chromosome copy-number changes confer stress-dependent adaptive advantages

Having established that balanced chromosomal rearrangements exert minimal effects on gene expression, we next asked whether different classes of structural variation influence fitness under stress. To address this, we assessed RED-Cas9 strains carrying balanced chromosomal rearrangements (MRS-g1, TRE-g1 and TRE-g5), extended LOH (MRS-g3, TRE-g3 and TRE-g4), or chromosome copy-number variations (MRS-g2, TRE-g2, TRE-g6 and TRE-g7*)* across a broad range of environmental and host-relevant conditions (Fig. 5; Supplemental_Fig_S13). These included growth at different temperatures (30 °C, 37 °C and 39 °C), pH (4.5 and 2.0), and glucose concentrations (2% and 0.2%), as well as under osmotic (1 M NaCl), oxidative (5 mM H_2O_2) and cell wall (10 mM caffeine) stress (Fig. 5A; Supplemental_Fig_S13). We also assessed susceptibility to the antifungal drugs fluconazole (Flc), amphotericin B (AmB) and caspofungin (Cas) (Fig. 5A-C; Supplemental_Fig_S14, Supplemental_Table_S11), filamentation on hypha-inducing media (Fig. 5D, Supplemental_Fig_S15), and virulence in the *Galleria mellonella* infection model (Fig. 5E; Supplemental_Fig_S15).

Strains carrying balanced chromosomal rearrangements showed no significant phenotypic differences from the parental strain across the conditions tested. Growth under the different stress conditions, antifungal susceptibility, filamentation and virulence were comparable to the parental SC5314 strain (Fig. 5A-E; Supplemental_Fig_S13, Supplemental_Fig_S14, Supplemental_Fig_S15). Similarly, strains carrying extended LOH showed few detectable

Downloaded from genome.cshlp.org on November 29, 2026 . Published by Cold Spring Harbor Laboratory Press

phenotypic differences from the parental strain despite exhibiting intermediate transcriptional changes by RNA-seq (Fig. 5A-E; Supplemental_Fig_S13, Supplemental_Fig_S14, Supplemental_Fig_S15). In contrast, strains carrying chromosome CNVs exhibited the strongest biological consequences. These effects were highly condition-specific, consistent with the pleiotropic effects of altered chromosome dosage. For example, MRS-g2 displayed reduced growth at elevated temperatures, increased sensitivity to caffeine and caspofungin and defective filamentation whereas TRE-g6 showed increased growth in caffeine but reduced growth in fluconazole (Fig. 5A-D; Supplemental_Fig_S13, Supplemental_Fig_S14, Supplemental_Fig_S15). TRE-g7 showed moderately increased growth during fluconazole growth curve analysis (Fig. 5A; Supplemental_Fig_S13) but grew in all tested fluconazole concentrations during MIC testing at 24 hours (Fig. 5C; Supplemental_Table_S11). The CNV group associated with altered colony morphology and reduced pathogenicity, primarily driven by MRS-g2 (Fig. 5E, Supplemental_Fig_S15). These results indicate that chromosome copy-number changes, rather than balanced chromosomal rearrangements or LOH, have the greatest impact on fitness across the conditions tested.

Given this distinction, we next asked whether selective pressure could drive the emergence of new chromosome copy-number changes in a balanced strain retaining Cas9 activity. We exposed MRS-g1(Cas9) to an inhibitory concentration of fluconazole and isolated a resistant derivative, MRS-g1(Cas9)R (Fig. 5F; Supplemental_Table_S11). Long-read ONT sequencing revealed that this resistant isolate had acquired an additional partial copy of ChrR, with a breakpoint mapping to MRS (Fig. 5G). This finding demonstrates that repeat-directed DNA cleavage can generate adaptive chromosome copy-number changes under antifungal selection.

Together, these findings demonstrate that the biological consequences of RED-Cas9-induced genome variation depend primarily on gene dosage rather than structural complexity. Balanced chromosomal rearrangements and LOH have little impact on fitness under the conditions examined, whereas chromosome copy-number changes generate both fitness costs and stress-dependent adaptive advantages.

Downloaded from genome.cshlp.org on November 29, 2026 . Published by Cold Spring Harbor Laboratory Press

DISCUSSION

Our study establishes repeat-directed CRISPR-Cas9 as an experimental approach to generate structural variation in *C. albicans* and to investigate the consequences of different classes of chromosomal rearrangement. Using this system, we show that balanced chromosomal rearrangements at repetitive loci have little detectable effect on gene expression or fitness, whereas chromosome copy-number changes account for most of the transcriptional and biological consequences of repeat-directed DNA damage. Alongside synthetic genome approaches (Dymond et al. 2011; Shen et al. 2016), CRISPR-Cas9 targeting of repetitive DNA has enabled the engineering of structural variation across diverse eukaryotes (Fleiss et al. 2019; Yadav et al. 2020; Liu et al. 2022; Qi et al. 2023).

In *C. albicans*, long repeats are associated with chromosomal rearrangements in clinical isolates, although the sources of DNA breaks at these loci remain unclear (Todd et al. 2019). Endogenous processes, including replication stress and R-loop formation, may contribute to this instability. This possibility is consistent with evidence that environmental stress can increase genome instability in *C. albicans* (Freire-Benéitez et al. 2016a; Forche et al. 2011). RED-Cas9 enables experimental investigation of the consequences of DNA breaks at native repeats by targeting multiple repeat copies while minimizing potential off-target effects (Supplemental_Table_S4). Although this approach may induce more simultaneous breaks than occur naturally, it enables direct comparison of balanced rearrangements, chromosome copy-number variants and LOH within an isogenic background. RED-Cas9 therefore complements studies using random or site-specific DNA damage (Hilton et al. 1985; Takagi et al. 2008; Feri et al. 2016; Marton et al. 2021) and approaches generating individual classes of structural variation (Després et al. 2025; Yang et al. 2021).

Our data demonstrated that balanced strains showed transcriptional profiles that closely resembled the parental strain and no detectable fitness differences across a wide range of environmental, antifungal and host-associated conditions. These findings contrast with observations in *S. cerevisiae*, where a single engineered reciprocal translocation altered

Downloaded from genome.cshlp.org on November 29, 2026 . Published by Cold Spring Harbor Laboratory Press

growth across multiple environmental conditions despite preserving gene content and dosage (Fleiss et al. 2019). They also differ from studies in metazoans showing that balanced rearrangements can alter transcription by modifying chromatin interactions, disrupting regulatory domains and repositioning genes within the nucleus (Sun et al. 2024; Harewood and Fraser 2014; Lupiáñez et al. 2015).

One explanation for this difference is the genomic context in which RED-Cas9 generates chromosome breaks. MRS and TRE elements are recombination-prone repetitive loci that frequently act as sites of chromosome exchange (Chibana and Magee 2009; Iwaguchi et al. 2004; Anderson et al. 2015; Freire-Benéitez et al. 2016b). Rearrangements occurring at these loci may therefore preserve local regulatory environments to a greater extent than rearrangements generated elsewhere in the genome. Although chromosome architecture remains poorly characterized in *C. albicans*, and we cannot currently test this model directly, our results raise the possibility that MRS and TRE repeats function as structural or chromatin boundaries loosely analogous to topologically associating domain (TAD) boundaries in metazoans (Bouwman et al. 2022; Paldi and Cavalli 2026). Under this model, rearrangements occurring precisely at MRS or TRE loci reposition large chromosomal blocks without exposing genes to new regulatory environments, which would explain why balanced rearrangements at these specific sites are transcriptionally neutral, unless the chromosomal context is changed. The experimental evolution data further support this interpretation. Balanced rearrangements remained stable during prolonged laboratory passaging and did not increase LOH frequency relative to the parental strain, indicating that they do not themselves generate a genetically unstable state. Instead, once formed, these rearrangements appear to represent stable chromosome configurations that are well tolerated during mitotic growth.

In contrast, chromosome copy-number changes had much greater biological consequences. Altered chromosome dosage produced widespread transcriptional changes consistent with gene-dosage effects and resulted in diverse, condition-dependent phenotypes, including altered antifungal susceptibility, impaired filamentation, reduced virulence and both fitness

Downloaded from genome.cshlp.org on November 29, 2026 . Published by Cold Spring Harbor Laboratory Press

costs and advantages depending on the environment. Furthermore, when an active RED-Cas9 strain was exposed to fluconazole, a resistant colony emerged carrying a partial duplication of ChrR, directly linking repeat-associated DNA damage to adaptive chromosome copy-number change. Together, these findings indicate that dosage-altering variants exert substantially greater effects on transcription and fitness than balanced chromosomal rearrangements, consistent with previous comparisons of euploid and aneuploid isolates (Mackey et al. 2025; Hirakawa et al. 2015; Yang et al. 2021).

With RED-Cas9, we generated three distinct classes of structural variant: balanced, LOH and CNV representing the outcomes of endogenous DNA damage at repeat loci. Our data suggest balanced rearrangements primarily occur via non-allelic homologous recombination (NAHR) between repeat copies. Segmental LOH events are predicted to occur via break-induced replication (BIR), as they extend to the telomere, unlike short gene-conversion tracts previously generated by targeting unique sites (Després et al. 2025). Segmental duplications may occur via template switching during BIR (Anand et al. 2014; Smith et al. 2007).

In addition to SVs with breakpoints at repeats, we also recovered strains with whole-chromosome ploidy changes, likely arising through multiple, non-exclusive mechanisms that nonetheless point to a consistent model. First, we detected these events only when Cas9 targeted repetitive DNA and not in strains expressing Cas9 without guide RNAs. This suggests that chromosome instability results from repeat-directed DNA cleavage rather than transformation or Cas9 expression alone. One possibility is that multiple double-strand breaks generated simultaneously at dispersed repeat loci overwhelm the repair machinery, allowing one or more chromosomes to enter mitosis with unresolved lesions, or aberrant repair products such as dicentric chromosomes, exacerbated in *C. albicans* by the uncoupling of DNA-damage and cell-cycle checkpoints (Loll-Krippleber et al. 2014). Persistent chromosome breaks are expected to promote chromosome missegregation, chromosome loss or sequestration into micronuclei and are increasingly recognized as direct consequences of on-target Cas9 cleavage in mammalian cells (Adikusuma et al. 2017; Leibowitz et al. 2021; Nahmad et al. 2022). Our findings parallel observations in *S.*

Downloaded from genome.cshlp.org on November 29, 2026 . Published by Cold Spring Harbor Laboratory Press

494 *cerevisiae*, where Cas9 targeting of Ty1 retrotransposons produced an increase in whole-
495 chromosome aneuploidy, including monosomies, trisomies and uniparental disomies (Qi et
496 al. 2023). The close similarity between these observations and the spectrum of ploidy
497 changes recovered here suggests that chromosome copy-number variation may represent a
498 general outcome of repeat-directed DNA cleavage rather than a species-specific response.
499 Additional mechanisms may further influence chromosome segregation in *C. albicans*. MRS
500 array size is an established determinant of mitotic nondisjunction (Lephart et al. 2005).
501 Because repair within tandem repeat arrays frequently results in repeat expansion or
502 contraction, repair of Cas9-induced breaks at MRS loci could alter array size and thereby
503 increase chromosome missegregation without producing a detectable structural
504 rearrangement. Once chromosome loss has occurred, monosomy can resolve through
505 duplication of the remaining homologue, restoring essential gene dosage while generating
506 chromosome-wide LOH (Todd et al. 2017).
507 How tetraploidy arose cannot be determined with certainty; however, we present two
508 mechanisms based on the available data. As with the aneuploidies, tetraploidy may have
509 arisen via unstable intermediate products of Cas9 action, which promote nuclear
510 missegregation and mitotic collapse, analogous to cancer evolution (Ganem et al. 2007;
511 Lens and Medema 2018). Intermediates may have involved the two trisomic chromosomes,
512 Chr4 and ChrR. In a second model, whole genome duplication arises from persistent cell-
513 cycle defects, potentially due to the segmental duplication. The pseudohyphal morphology
514 and aberrant nuclear numbers are indicative of cell-cycle defects (Bachewich et al. 2005;
515 Bachewich and Whiteway 2005; Finley et al. 2008) and such structures resemble trimeras
516 which have been previously shown to generate aneuploidy via a tetraploid intermediate
517 during *C. albicans* antifungal drug adaptation (Harrison et al. 2014). Whether these defects
518 led to the tetraploidy or simply result from it is unclear; ploidy itself alters cell cycle
519 progression and filamentation in *S. cerevisiae* (Galitski et al. 1999). From either mechanism,
520 sustained mitotic instability could then promote further chromosome loss from the tetraploid,
521 analogous to either concerted chromosome loss in the parasexual cycle (Bennett and

Downloaded from genome.cshlp.org on November 29, 2026 . Published by Cold Spring Harbor Laboratory Press

Johnson 2003; Forche et al. 2008), during fluconazole evolution (Harrison et al. 2014) or in tetraploid *S. cerevisiae* (Storchová et al. 2006).

Although our data do not distinguish between possible mechanisms for whole chromosome and whole genome CNV, they support a model in which repeat-directed DNA cleavage promotes chromosome instability through multiple, non-mutually exclusive mechanisms. This instability generates dosage variation that, while potentially costly in stable environments, provides population heterogeneity to facilitate rapid adaptation under selective pressure such as antifungal drug exposure (Selmecki et al. 2015).

Together, our results establish RED-Cas9 as a tractable experimental platform for generating structural variation in *C. albicans* and for dissecting the independent contributions of balanced rearrangements, chromosome copy-number changes and LOH to genome plasticity. More broadly, our findings demonstrate that the biological consequences of structural variation depend primarily on genome balance rather than chromosome rearrangement itself. By experimentally separating these distinct classes of genome variation, RED-Cas9 provides a framework for understanding how chromosome architecture and dosage contribute to adaptation in fungal pathogens.

METHODS

Yeast strains and growth conditions

All strains used in this study are listed in Supplemental_Table_S12. Routine culturing was performed at 30 °C in Yeast Extract–Peptone–Dextrose (YPD) medium, prepared as 1% yeast extract (Melford), 2% Bacto peptone (BD), and 2% dextrose (Fisher Chemical), supplemented with 0.1 mg/mL adenine and 0.08 mg/mL uridine (Sigma). When required, YPD was supplemented with antifungal drugs or stress-inducing compounds as described in the Supplemental Methods.

RED-Cas9 system

The RED-Cas9 system was used to induce genome rearrangements at Major Repeat Sequence (MRS) and Telomere-Associated Repeat Element (TRE) loci. Single-guide RNAs were designed to target the RB2 and RPS components of the MRS, TRE elements, or

Downloaded from genome.cshlp.org on November 29, 2026 . Published by Cold Spring Harbor Laboratory Press

omitted in NG strains (Supplemental_Table_S13). A previously described cloning-free CRISPR–Cas9 system was used (Nguyen et al. 2017), and no exogenous repair template was provided. Transformants were selected on nourseothricin. TRE-targeted strains were initially screened by PCR using primers targeting *TLO34* (AB1220 and AB1221; Supplemental_Table_S13) and subsequently analyzed by CHEF electrophoresis. Due to the repetitive nature and length of the locus, MRS-targeted strains were screened exclusively by CHEF electrophoresis (Supplemental_Table_S1). Further details, primers (Supplemental_Table_S13), plasmids and cassette components (Supplemental_Table_S14) are listed in Supplemental Methods.

CHEF gel electrophoresis

Chromosomal karyotypes were analyzed by contour-clamped homogeneous electric field (CHEF) gel electrophoresis following established protocols (Schwartz and Cantor 1984) with minor modifications as we have previously reported (Rizzo et al. 2022). Intact chromosomal DNA was embedded in low-melt agarose plugs (BioRad), separated by pulsed-field electrophoresis (CHEF-DR II system, 14 °C, 0.5× TBE, Block 1: 60–120 s, 6 V/cm, 12 h; Block 2: 120–300 s, 4.5–5 V/cm, 26 h), stained with ethidium bromide and imaged with a Syngene GBox Chemi XX6 system.

Karyotype stability

To assess karyotype stability in balanced RED-Cas9 strains MRS-g1 and TRE-g5, glycerol stocks were struck onto YPD agar. Nine single colonies were then re-struck after 48 hours at 30 °C onto fresh plates. These nine independent evolutions were then passaged every 48 hours, each time taking the distinct colony closest to the center of the plate to be as random as possible. After ten passages, colonies were assessed by CHEF electrophoresis, with the parental strain as a reference.

Flow cytometry

Genome ploidy was estimated by propidium iodide staining and flow cytometry as previously described (Todd et al. 2018). Samples were prepared in biological triplicate, and fluorescence intensity distributions were used to quantify polyploidy. Statistical analyses

Downloaded from genome.cshlp.org on November 29, 2026 . Published by Cold Spring Harbor Laboratory Press

were performed in R, with full gating and analysis procedures described in the Supplemental Methods.

Genomic sequencing

Genomic DNA was extracted from logarithmically growing cultures using commercial kits. Oxford Nanopore libraries were prepared using ligation-based workflows and sequenced on GridION platforms, while Illumina libraries were prepared using PCR-free methods and sequenced using paired-end 150 bp chemistry. Detailed library preparation, sequencing, and quality control procedures are described in the Supplemental Methods.

RNA sequencing

RNA sequencing was performed on MRS and TRE strains in separate sequencing rounds, each including SC5314 wild-type controls to which they were compared. RNA was extracted from exponentially growing cultures in YPD at 30 °C, and libraries were prepared using strand-specific workflows with either poly(A) enrichment or rRNA depletion. Sequencing was performed using paired-end 150 bp chemistry. Detailed library preparation and quality control procedures are provided in the Supplemental Methods.

Quantitative PCR analysis

Quantitative PCR primers targeting single-copy BUSCO genes were designed with one primer pair per chromosome (Supplemental_Table_S13). Genomic DNA was extracted using a standard yeast protocol, and qPCR was performed using SYBR-based chemistry. Chromosome dosage was calculated using ΔΔCt-based approaches relative to SC5314. Detailed cycling conditions, filtering criteria, and statistical analyses are provided in the Supplemental Methods.

Loss-of-heterozygosity assay

To establish LOH rates in SC5314 compared to RED-Cas9 strains, 5-FOA assays were performed, based on established protocols (Forche et al. 2011; Avramovska and Hickman 2019). *URA3/ura3Δ::NAT1* strains were generated and 12 colonies were selected per strain,

Downloaded from genome.cshlp.org on November 29, 2026 . Published by Cold Spring Harbor Laboratory Press

cultured in YPD and plated onto YPD and SC 0.1% 5-FOA plates at suitable dilutions. Colony counts were analyzed in R (R Core Team 2024) to provide estimated the LOH rate per strain. Full methods are available in Supplemental Methods.

Bioinformatics

Structural genome analysis primarily used Oxford Nanopore Technologies long-read data. Genomes were initially screened for structural variation with assembly-dependent methods. Assembly completeness was assessed with BUSCO (Manni et al. 2021). To resolve structurally heterozygous karyotypes, assembly-independent analyses were performed, using established tools and custom scripts, and included structural variant detection, breakpoint analysis, MRS length, karyotype reconstruction, loss-of-heterozygosity, copy-number and DSB repair pathway analyses. Small variant analysis of Illumina whole genome sequencing was performed with GATK HaplotypeCaller (McKenna et al. 2010) and tested for enrichment in CRISPRitz predicted off-target sites (Cancellieri et al. 2020). Differential expression analysis was performed with DESeq2 (Love et al. 2014). Complete software versions, parameters, filtering thresholds, and custom scripts are described in the Supplemental Methods. Statistical analyses were primarily performed in R (R Core Team 2024). Custom scripts used for genomic, transcriptomic and phenotypic analyses are provided as Supplemental Code.

Growth curves

Growth curve analysis was used to assess baseline fitness, and screen stress-specific fitness. These were performed under clinically relevant stress conditions, including temperature, acidic pH, low glucose, osmotic stress, oxidative stress and antifungal drugs. Stress specific fitness was estimated by normalizing growth under stress to the non-stress baseline. Further details are provided in the Supplemental Methods.

Microplate dilution assays

Sensitivity to fluconazole, amphotericin B and caspofungin was assessed by microdilution minimum inhibitory concentration (MIC) assays in YPD. Cultures were inoculated into 96-well plates containing serial dilutions of antifungal drugs and incubated at 30 °C. Growth was

Downloaded from genome.cshlp.org on November 29, 2026 . Published by Cold Spring Harbor Laboratory Press

measured by OD_{600} at 24 h intervals and data were analyzed in R. Full assay conditions and analysis procedures are provided in the Supplemental Methods.

Filamentation assay

Filamentation was induced using RPMI medium or Spider medium, with or without 2% agar. For colony analysis, strains were plated to yield approximately 20 CFU per plate and incubated at 37 °C for five days. Image analysis and statistical procedures are described in the Supplemental Methods.

Microscopy and image analysis

Cell morphology and nuclear organization were assessed by fluorescence microscopy following fixation and staining. Cells were subcultured in relevant media (YPD, Spider, or RPMI) and incubated at either 30 °C or 37 °C, and then fixed, stained, and imaged by confocal microscopy. Statistical analyses were performed in R. Full staining protocols, imaging parameters, classification criteria, and statistical models are described in the Supplemental Methods.

Pathogenicity testing

Pathogenicity was assessed using the *Galleria mellonella* infection model following the protocol described by Li et al. (2013). Larvae were injected with 2×10□ CFU of *C. albicans* per larva, with PBS-injected and non-injected controls. Mortality was monitored over seven days at 37 °C across three biological replicates (n = 20 per replicate; minimum 57 larvae per condition after exclusion of damaged individuals). Analysis detailed in Supplemental Methods.

Fluconazole evolution

RED-Cas9 strains were plated at approximately 200 CFU onto YPD and 500 CFU onto YPD supplemented with 8 µg/mL fluconazole and incubated for five days (two days YPD). Single colonies were isolated, expanded, and passaged three times in 96-well plates containing YPD. Passaged cultures were then diluted into YPD supplemented with 16 µg/mL fluconazole, and growth curves were performed. For each strain, the two fastest-growing

Downloaded from genome.cshlp.org on November 29, 2026 . Published by Cold Spring Harbor Laboratory Press

659 derivatives at 24 hours were selected for further analysis by CHEF electrophoresis and
660 minimum inhibitory concentration (MIC) assays.

661 **DATA ACCESS**

662 All raw sequence data generated in this study (Oxford Nanopore and Illumina genomic
663 sequencing, and RNA sequencing) have been submitted to the NCBI BioProject database
664 (https://www.ncbi.nlm.nih.gov/bioproject/) under accession number PRJNA1377917. Custom
665 scripts are available as Supplemental Code, on GitHub (https://github.com/M-A-
666 Shaw/Candida_RED-Cas9_analysis) and on Zenodo
667 (https://doi.org/10.5281/zenodo.23872942).

668

669 **COMPETING INTEREST STATEMENT**

670 The authors declare no competing interests.

671

672 **ACKNOWLEDGEMENT**

673 We thank the Kent Fungal Group, members of the Buscaino Lab and the Selmecki Lab, and
674 Alison Pidoux for insightful discussions and for critically reading the manuscript. Funding
675 was provided by the BBSRC: MS was funded by the South Coast Biosciences Doctoral
676 Training Partnership code BB/T008768/1, SVE under the grant ‘Epigenetics of stress-
677 induced genome instability in the human fungal pathogen’, code BB/T006315/1.

678 **AUTHOR CONTRIBUTIONS**

679 MS designed and performed wet-lab experiments, carried out the majority of the
680 bioinformatics analyses, and co-wrote the manuscript. SVE contributed to experimental
681 design, performed wet-lab experiments, conducted bioinformatics analyses, and drafted the
682 initial manuscript. RJP generated long-read sequencing data, performed bioinformatics
683 analyses, and provided comments on the manuscript draft. CU assisted with the karyotype
684 analyses by CHEF electrophoresis. JD performed PI staining and flow cytometry for NG

Downloaded from genome.cshlp.org on November 29, 2026 . Published by Cold Spring Harbor Laboratory Press

685 strains. AB conceived and designed the project, supervised all aspects of the work, and
686 wrote the manuscript.

Downloaded from genome.cshlp.org on November 29, 2026 . Published by Cold Spring Harbor Laboratory Press

REFERENCES

Adikusuma F, Williams N, Grutzner F, Hughes J, Thomas P. 2017. Targeted deletion of an entire chromosome using CRISPR/Cas9. *Mol Ther* 25: 1736–1738.

Anand RP, Tsaponina O, Greenwell PW, Lee CS, Du W, Petes TD, Haber JE. 2014. Chromosome rearrangements via template switching between diverged repeated sequences. *Genes Dev* 28: 2394–2406.

Anderson FM, Visser ND, Amses KR, Hodgins-Davis A, Weber AM, Metzner KM, McFadden MJ, Mills RE, O'Meara MJ, James TY, et al. 2023. *Candida albicans* selection for human commensalism results in substantial within-host diversity without decreasing fitness for invasive disease. *PLoS Biol* 21: e3001822.

Anderson MZ, Dietz SM. 2024. Evolution and strain diversity advance exploration of *Candida albicans* biology. *mSphere* 9: e00641-23.

Anderson MZ, Saha A, Haseeb A, Bennett RJ. 2017. A chromosome 4 trisomy contributes to increased fluconazole resistance in a clinical isolate of *Candida albicans*. *Microbiology* 163: 856–865.

Anderson MZ, Wigen LJ, Burrack LS, Berman J. 2015. Real-time evolution of a subtelomeric gene family in *Candida albicans*. *Genetics* 200: 907–919.

Asakura K, Iwaguchi S, Homma M, Sukai T, Higashide K, Tanaka K. 1991. Electrophoretic karyotypes of clinically isolated yeasts of *Candida albicans* and *C. glabrata*. *J Gen Microbiol* 137: 2531–2538.

Avramovska O, Hickman MA. 2019. The magnitude of *Candida albicans* stress-induced genome instability results from an interaction between ploidy and antifungal drugs. *G3 (Bethesda)* 9: 4019–4027.

Bachewich C, Mantel A, Whiteway M. 2005. Cell cycle arrest during S or M phase generates polarized growth via distinct signals in *Candida albicans*. *Mol Microbiol* 57: 942–959.

Downloaded from genome.cshlp.org on November 29, 2026 . Published by Cold Spring Harbor Laboratory Press

712 Bachewich C, Whiteway M. 2005. Cyclin Cln3p links G1 progression to hyphal and
713 pseudohyphal development in *Candida albicans*. *Eukaryot Cell* 4: 95–102.

714 Beach RR, Ricci-Tam C, Brennan CM, Moomau CA, Hsu P-H, Hua B, Silberman RE,
715 Springer M, Amon A. 2017. Aneuploidy causes non-genetic individuality. *Cell* 169: 229–
716 242.e21.

717 Beekman CN, Ene IV. 2020. Short-term evolution strategies for host adaptation and drug
718 escape in human fungal pathogens. *PLoS Pathog* 16: e1008519.

719 Ben-David U, Amon A. 2020. Context is everything: aneuploidy in cancer. *Nat Rev Genet* 21:
720 44–62.

721 Bennett RJ, Johnson AD. 2003. Completion of a parasexual cycle in *Candida albicans* by
722 induced chromosome loss in tetraploid strains. *EMBO J* 22: 2505–2515.

723 Bouwman BAM, Crosetto N, Bienko M. 2022. The era of 3D and spatial genomics. *Trends*
724 *Genet* 38: 1062–1075.

725 Butler G, Rasmussen MD, Lin MF, Santos MAS, Sakthikumar S, Munro CA, Rheinbay E,
726 Grabherr M, Forche A, Reedy JL, et al. 2009. Evolution of pathogenicity and sexual
727 reproduction in eight Candida genomes. *Nature* 459: 657–662.

728 Cancellieri S, Canver MC, Bombieri N, Giugno R, Pinello L. 2020. CRISPRitz: rapid, high-
729 throughput and variant-aware in silico off-target site identification for CRISPR genome
730 editing. *Bioinformatics* 36: 2001–2008.

731 Chibana H, Beckerman JL, Magee PT. 2000. Fine-resolution physical mapping of genomic
732 diversity in *Candida albicans*. *Genome Res* 10: 1865–1877.

733 Chibana H, Magee BB, Grindle S, Ran Y, Scherer S, Magee PT. 1998. A physical map of
734 chromosome 7 of *Candida albicans*. *Genetics* 149: 1739–52.

Downloaded from genome.cshlp.org on November 29, 2026 . Published by Cold Spring Harbor Laboratory Press

735 Chibana H, Magee PT. 2009. The enigma of the major repeat sequence of *Candida albicans*.
736 *Future Microbiol* 4: 171–9.

737 Chu W-S, Magee BB, Magee PT, Sadhu C, McEachern MJ, Rustchenko-Bulgac EP, Schmid
738 J, Soll DR, Hicks JB. 1993. Construction of an SfiI macrorestriction map of the *Candida*
739 *albicans* genome. *J Bacteriol* 175: 6637–6651.

740 Ciudad T, Hickman M, Bellido A, Berman J, Larriba G. 2016. Phenotypic consequences of a
741 spontaneous loss of heterozygosity in a common laboratory strain of *Candida albicans*.
742 *Genetics* 203: 1161–1176.

743 Cravener MV, Do E, May G, Zarnowski R, Andes DR, McManus CJ, Mitchell AP. 2023.
744 Reinforcement amid genetic diversity in the *Candida albicans* biofilm regulatory network.
745 *PLoS Pathog* 19: e1011109.

746 Denning DW. 2024. Global incidence and mortality of severe fungal disease. *Lancet Infect*
747 *Dis* 24: e428–e438.

748 Després PC, Gervais NC, Fogal M, Rogers RKJ, Cuomo CA, Shapiro RS. 2025. Targeted
749 loss of heterozygosity in *Candida albicans* using CRISPR-Cas9 reveals the functional impact
750 of allelic variation. *Genetics* 231: iyaf154.

751 Dunn MJ, Anderson MZ. 2019. To repeat or not to repeat: repetitive sequences regulate
752 genome stability in *Candida albicans*. *Genes (Basel)* 10: 866.

753 Dunn MJ, Shazib SUA, Simonton E, Slot JC, Anderson MZ. 2022. Architectural groups of a
754 subtelomeric gene family evolve along distinct paths in *Candida albicans*. *G3 (Bethesda)* 12:
755 jkac283.

756 Dymond JS, Richardson SM, Coombes CE, Babatz T, Muller H, Annaluru N, Blake WJ,
757 Schwerzmann JW, Dai J, Lindstrom DL, et al. 2011. Synthetic chromosome arms function in
758 yeast and generate phenotypic diversity by design. *Nature* 477: 471–476.

Downloaded from genome.cshlp.org on November 29, 2026 . Published by Cold Spring Harbor Laboratory Press

759 Ene IV, Bennett RJ, Anderson MZ. 2019. Mechanisms of genome evolution in *Candida*
760 *albicans*. *Curr Opin Microbiol* 52: 47–54.

761 Ene IV, Farrer RA, Hirakawa MP, Agwamba K, Cuomo CA, Bennett RJ. 2018. Global
762 analysis of mutations driving microevolution of a heterozygous diploid fungal pathogen. *Proc*
763 *Natl Acad Sci* 115: E8688–E8697.

764 Evans C, Hardin J, Stoebel DM. 2017. Selecting between-sample RNA-seq normalization
765 methods from the perspective of their assumptions. *Brief Bioinform* 19: 776–792.

766 Feri A, Loll-Krippleber R, Commere PH, Maufrais C, Sertour N, Schwartz K, Sherlock G,
767 Bougnoux ME, d'Enfert C, Legrand M. 2016. Analysis of repair mechanisms following an
768 induced double-strand break uncovers recessive deleterious alleles in the *Candida albicans*
769 diploid genome. *mBio* 7: e01109-16.

770 Finley KR, Bouchonville KJ, Quick A, Berman J. 2008. Dynein-dependent nuclear dynamics
771 affect morphogenesis in *Candida albicans* by means of the Bub2p spindle checkpoint. *J Cell*
772 *Sci* 121: 466–476.

773 Flanagan PR, Fletcher J, Boyle H, Sulea R, Moran GP, Sullivan DJ. 2018. Expansion of the
774 TLO gene family enhances the virulence of *Candida* species. *PLoS One* 13: e0200852.

775 Fleiss A, O'Donnell S, Fournier T, Lu W, Agier N, Delmas S, Schachere J, Fischer G. 2019.
776 Reshuffling yeast chromosomes with CRISPR/Cas9. *PLoS Genet* 15: e1008332.

777 Fletcher J, O'Connor-Moneley J, Frawley D, Flanagan PR, Alaalm L, Menendez-Manjon P,
778 Estevez SV, Hendricks S, Woodruff AL, Buscaino A, et al. 2023. Deletion of the *Candida*
779 *albicans* TLO gene family using CRISPR-Cas9 mutagenesis allows characterisation of
780 functional differences in α-, β- and γ- TLO gene function. *PLoS Genet* 19: e1011082.

781 Forche A, Abbey D, Pisithkul T, Weinzierl MA, Ringstrom T, Bruck D, Petersen K, Berman J.
782 2011. Stress alters rates and types of loss of heterozygosity in *Candida albicans*. *mBio* 2:
783 e00129-11.

Downloaded from genome.cshlp.org on November 29, 2026 . Published by Cold Spring Harbor Laboratory Press

784 Forche A, Alby K, Schaefer D, Johnson AD, Berman J, Bennett RJ. 2008. The parasexual
785 cycle in *Candida albicans* provides an alternative pathway to meiosis for the formation of
786 recombinant strains. *PLoS Biol* 6: e110.

787 Forche A, Magee PT, Selmecki A, Berman J, May G. 2009. Evolution in *Candida albicans*
788 populations during a single passage through a mouse host. *Genetics* 182: 799–811.

789 Ford CB, Funt JM, Abbey D, Issi L, Guiducci C, Martinez DA, Delorey T, Li BY, White T,
790 Cuomo C, et al. 2015. The evolution of drug resistance in clinical isolates of *Candida*
791 *albicans*. *eLife* 4: e00662.

792 Freire-Benéitez V, Gourlay S, Berman J, Buscaino A. 2016a. Sir2 regulates stability of
793 repetitive domains differentially in the human fungal pathogen *Candida albicans*. *Nucleic*
794 *Acids Res* 44: 9166–9179.

795 Freire-Benéitez V, Price RJ, Tarrant D, Berman J, Buscaino A. 2016b. *Candida albicans*
796 repetitive elements display epigenetic diversity and plasticity. *Sci Rep* 6: 22989.

797 Galitski T, Saldanha AJ, Styles CA, Lander ES, Fink GR. 1999. Ploidy regulation of gene
798 expression. *Science* 285: 251–254.

799 Ganem NJ, Storchova Z, Pellman D. 2007. Tetraploidy, aneuploidy and cancer. *Curr Opin*
800 *Genet Dev* 17: 157–162.

801 Haran J, Boyle H, Hokamp K, Yeomans T, Liu Z, Church M, Fleming AB, Anderson MZ,
802 Berman J, Myers LC, et al. 2014. Telomeric ORFs (TLOs) in *Candida* spp. encode Mediator
803 subunits that regulate distinct virulence traits. *PLoS Genet* 10: e1004658.

804 Harewood L, Fraser P. 2014. The impact of chromosomal rearrangements on regulation of
805 gene expression. *Hum Mol Genet* 23: R76–R85.

806 Harewood L, Schütz F, Boyle S, Perry P, Delorenzi M, Bickmore WA, Reymond A. 2010. The
807 effect of translocation-induced nuclear reorganization on gene expression. *Genome Res* 20:
808 554–564.

Downloaded from genome.cshlp.org on November 29, 2026 . Published by Cold Spring Harbor Laboratory Press

Harrison BD, Hashemi J, Bibi M, Pulver R, Bavli D, Nahmias Y, Wellington M, Sapiro G, Berman J. 2014. A tetraploid intermediate precedes aneuploid formation in yeasts exposed to fluconazole. *PLoS Biol* 12: e1001815.

Hilton C, Markie D, Corner B, Rikkerink E, Poulter R. 1985. Heat shock induces chromosome loss in the yeast *Candida albicans*. *Mol Gen Genet* 200: 162–168.

Hirakawa MP, Chyou DE, Huang D, Slan AR, Bennett RJ. 2017. Parasex generates phenotypic diversity de novo and impacts drug resistance and virulence in *Candida albicans*. *Genetics* 207: 1195–1211.

Hirakawa MP, Martinez DA, Sakthikumar S, Anderson MZ, Berlin A, Gujja S, Zeng Q, Zisson E, Wang JM, Greenberg JM, et al. 2015. Genetic and phenotypic intra-species variation in *Candida albicans*. *Genome Res* 25: 413–425.

Hitzler SUJ, Fernández-Fernández C, Montaño DE, Dietschmann A, Gresnigt MS. 2025. Microbial adaptive pathogenicity strategies to the host inflammatory environment. *FEMS Microbiol Rev* 49: fuae032.

Hou J, Shi X, Chen C, Soliman Islam M, Johnson AF, Kanno T, Huettel B, Yen MR, Hsu FM, Ji T, et al. 2018. Global impacts of chromosomal imbalance on gene expression in *Arabidopsis* and other taxa. *Proc Natl Acad Sci* 115: E11321–E11330.

Hoyer LL, Freeman BA, Hogan EK, Hernandez AG. 2024. Use of a *Candida albicans* SC5314 PacBio HiFi reads dataset to close gaps in the reference genome assembly, reveal a subtelomeric gene family, and produce accurate phased allelic sequences. *Front Cell Infect Microbiol* 14: 1329438.

Iracane E, Arias-Sardá C, Maufrais C, Ene IV, d'Enfert C, Buscaino A. 2024. Identification of an active RNAi pathway in *Candida albicans*. *Proc Natl Acad Sci* 121: e2315926121.

Iwaguchi SI, Homma M, Chibana H, Tanaka K. 1992. Isolation and characterization of a repeated sequence (RPS1) of *Candida albicans*. *J Gen Microbiol* 138: 1893–1900.

Downloaded from genome.cshlp.org on November 29, 2026 . Published by Cold Spring Harbor Laboratory Press

834 Iwaguchi SI, Sato M, Magee BB, Magee PT, Makimura K, Suzuki T. 2001. Extensive
835 chromosome translocation in a clinical isolate showing the distinctive carbohydrate
836 assimilation profile from a candidiasis patient. *Yeast* 18: 1035–1046.

837 Iwaguchi SI, Suzuki M, Sakai N, Nakagawa Y, Magee PT, Suzuki T. 2004. Chromosome
838 translocation induced by the insertion of the URA blaster into the major repeat sequence
839 (MRS) in *Candida albicans*. *Yeast* 21: 619–634.

840 Jackson AP, Gamble JA, Yeomans T, Moran GP, Saunders D, Harris D, Aslett M, Barrell JF,
841 Butler G, Citiulo F, et al. 2009. Comparative genomics of the fungal pathogens *Candida*
842 *dubliniensis* and *Candida albicans*. *Genome Res* 19: 2231–2244.

843 Leibowitz ML, Papathanasiou S, Doerfler PA, Blaine LJ, Sun L, Yao Y, Zhang CZ, Weiss MJ,
844 Pellman D. 2021. Chromothripsis as an on-target consequence of CRISPR-Cas9 genome
845 editing. *Nat Genet* 53: 895–905.

846 Lens SMA, Medema RH. 2018. Cytokinesis defects and cancer. *Nat Rev Cancer* 19: 32–45.

847 Lephart PR, Chibana H, Magee PT. 2005. Effect of the major repeat sequence on
848 chromosome loss in *Candida albicans*. *Eukaryot Cell* 4: 733–741.

849 Lephart PR, Magee PT. 2006. Effect of the major repeat sequence on mitotic recombination
850 in *Candida albicans*. *Genetics* 174: 1737–1744.

851 Li D-D, Deng L, Hu G-H, Zhao L-X, Hu D-D, Jiang Y-Y, Wang Y. 2013. Using *Galleria*
852 *mellonella-Candida albicans* infection model to evaluate antifungal agents. *Biol Pharm Bull*
853 36: 1482–1487.

854 Li X, Brock GN, Rouchka EC, Cooper NGF, Wu D, O'Toole TE, Gill RS, Eteleeb AM, O'Brien
855 L, Rai SN. 2017. A comparison of per sample global scaling and per gene normalization
856 methods for differential expression analysis of RNA-seq data. *PLoS One* 12: e0176185.

Downloaded from genome.cshlp.org on November 29, 2026 . Published by Cold Spring Harbor Laboratory Press

857 Liang SH, Anderson MZ, Hirakawa MP, Wang JM, Frazer C, Alaalm LM, Thomson GJ, Ene
858 IV, Bennett RJ. 2019. Hemizygosity enables a mutational transition governing fungal
859 virulence and commensalism. *Cell Host Microbe* 25: 418–431.e6.

860 Liang SH, Bennett RJ. 2019. The impact of gene dosage and heterozygosity on the diploid
861 pathobiont *Candida albicans*. *J Fungi* 6: 10.

862 Liu Y, Ma G, Gao Z, Li J, Wang J, Zhu X, Ma R, Yang J, Zhou Y, Hu K, et al. 2022. Global
863 chromosome rearrangement induced by CRISPR-Cas9 reshapes the genome and
864 transcriptome of human cells. *Nucleic Acids Res* 50: 3456–3474.

865 Loll-Krippleber R, d'Enfert C, Feri A, Diogo D, Perin A, Marcet-Houben M, Bougnoux ME,
866 Legrand M. 2014. A study of the DNA damage checkpoint in *Candida albicans*: uncoupling of
867 the functions of Rad53 in DNA repair, cell cycle regulation and genotoxic stress-induced
868 polarized growth. *Mol Microbiol* 91: 452–471.

869 Love MI, Huber W, Anders S. 2014. Moderated estimation of fold change and dispersion for
870 RNA-seq data with DESeq2. *Genome Biol* 15: 550.

871 Lupiáñez DG, Kraft K, Heinrich V, Krawitz P, Brancati F, Klopocki E, Horn D, Kayserili H,
872 Opitz JM, Laxova R, et al. 2015. Disruptions of topological chromatin domains cause
873 pathogenic rewiring of gene-enhancer interactions. *Cell* 161: 1012–1025.

874 Mackey AI, Fillinger RJ, Hendricks PS, Thomson GJ, Cuomo CA, Bennett RJ, Anderson MZ.
875 2025. Aneuploidy confers a unique transcriptional and phenotypic profile to *Candida*
876 *albicans*. *Nat Commun* 16: 3287.

877 Magee BB, D'Souza TM, Magee PT. 1987. Strain and species identification by restriction
878 fragment length polymorphisms in the ribosomal DNA repeat of *Candida* species. *J Bacteriol*
879 169: 1639–43.

880 Magee PT. 1993. Variations in chromosome size and organization in *Candida albicans* and
881 *Candida stellatoidea*. *Trends Microbiol* 1: 338–342.

Downloaded from genome.cshlp.org on November 29, 2026 . Published by Cold Spring Harbor Laboratory Press

882 Manni M, Berkeley MR, Seppey M, Simão FA, Zdobnov EM. 2021. BUSCO update: novel
883 and streamlined workflows along with broader and deeper phylogenetic coverage for scoring
884 of eukaryotic, prokaryotic, and viral genomes. *Mol Biol Evol* 38: 4647–4654.

885 Marton T, Chauvel M, Feri A, Maufrais C, d'Enfert C, Legrand M. 2021. Factors that influence
886 bidirectional long-tract homozygosis due to double-strand break repair in *Candida albicans*.
887 *Genetics* 218: iyab028.

888 McKenna A, Hanna M, Banks E, Sivachenko A, Cibulskis K, Kernytsky A, Garimella K,
889 Altshuler D, Gabriel S, Daly M, et al. 2010. The Genome Analysis Toolkit: a MapReduce
890 framework for analyzing next-generation DNA sequencing data. *Genome Res* 20: 1297–
891 1303.

892 Muenzner J, Trébulle P, Agostini F, Zauber H, Messner CB, Steger M, Kilian C, Lau K,
893 Barthel N, Lehmann A, et al. 2024. Natural proteome diversity links aneuploidy tolerance to
894 protein turnover. *Nature* 630: 149–157.

895 Muzzey D, Sherlock G, Weissman JS. 2014. Extensive and coordinated control of allele-
896 specific expression by both transcription and translation in *Candida albicans*. *Genome Res*
897 24: 963–973.

898 Nahmad AD, Reuveni E, Goldschmidt E, Tenne T, Liberman M, Horovitz-Fried M, Khosravi
899 R, Kobo H, Reinstein E, Madi A, et al. 2022. Frequent aneuploidy in primary human T cells
900 after CRISPR-Cas9 cleavage. *Nat Biotechnol* 40: 1807–1812.

901 Nguyen N, Quail MMF, Hernday AD. 2017. An efficient, rapid, and recyclable system for
902 CRISPR-mediated genome editing in *Candida albicans*. *mSphere* 2: e00149-17.

903 Oggenfuss U, Todd RT, Soisangwan N, Kemp B, Guyer A, Beach A, Selmecki A. 2025.
904 *Candida albicans* isolates contain frequent heterozygous structural variants and
905 transposable elements within genes and centromeres. *Genome Res* 35: 824–838.

Downloaded from genome.cshlp.org on November 29, 2026 . Published by Cold Spring Harbor Laboratory Press

906 Paldi F, Cavalli G. 2026. 3D genome folding in epigenetic regulation and cellular memory.
907 *Trends Cell Biol* 36: 28–41.

908 Qi L, Sui Y, Tang XX, McGinty RJ, Liang XZ, Dominska M, Zhang K, Mirkin SM, Zheng DQ,
909 Petes TD. 2023. Shuffling the yeast genome using CRISPR/Cas9-generated DSBs that
910 target the transposable Ty1 elements. *PLoS Genet* 19: e1010590.

911 R Core Team. 2024. R: a language and environment for statistical computing. R Foundation
912 for Statistical Computing, Vienna, Austria. https://www.R-project.org/.

913 Ran FA, Hsu PD, Wright J, Agarwala V, Scott DA, Zhang F. 2013. Genome engineering
914 using the CRISPR-Cas9 system. *Nat Protoc* 8: 2281–2308.

915 Rizzo M, Soisangwan N, Vega-Estevez S, Price RJ, Uyl C, Iracane E, Shaw M, Soetaert J,
916 Selmecki A, Buscaino A. 2022. Stress combined with loss of the *Candida albicans* SUMO
917 protease Ulp2 triggers selection of aneuploidy via a two-step process. *PLoS Genet* 18:
918 e1010576.

919 Ropars J, Maufrais C, Diogo D, Marcet-Houben M, Perin A, Sertour N, Mosca K, Permal E,
920 Laval G, Bouchier C, et al. 2018. Gene flow contributes to diversification of the major fungal
921 pathogen *Candida albicans*. *Nat Commun* 9: 2253.

922 Rustchenko E. 2007. Chromosome instability in *Candida albicans*. *FEMS Yeast Res* 7: 2–11.

923 Schille TB, Sprague JL, Naglik JR, Brunke S, Hube B. 2025. Commensalism and
924 pathogenesis of *Candida albicans* at the mucosal interface. *Nat Rev Microbiol* 23: 525–540.

925 Schwartz DC, Cantor CR. 1984. Separation of yeast chromosome-sized DNAs by pulsed
926 field gradient gel electrophoresis. *Cell* 37: 67–75.

927 Scott NE, Zhou X, Wash E, Zajac C, Kline SE, Schmidt SE, Selmecki A. 2026. Aneuploidy,
928 polyploidy and loss of heterozygosity distinguish serial bloodstream isolates of *Candida*
929 *albicans*. *Microb Genom* 12: 001659.

Downloaded from genome.cshlp.org on November 29, 2026 . Published by Cold Spring Harbor Laboratory Press

930 Selmecki A, Forche A, Berman J. 2006. Aneuploidy and isochromosome formation in drug-
931 resistant *Candida albicans*. *Science* 313: 367–70.

932 Selmecki A, Forche A, Berman J. 2010. Genomic plasticity of the human fungal pathogen
933 *Candida albicans*. *Eukaryot Cell* 9: 991–1008.

934 Selmecki AM, Maruvka YE, Richmond PA, Guillet M, Shoresh N, Sorenson AL, De S,
935 Kishony R, Michor F, Dowell R, et al. 2015. Polyploidy can drive rapid adaptation in yeast.
936 *Nature* 519: 349–352.

937 Shen Y, Stracquadanio G, Wang Y, Yang K, Mitchell LA, Xue Y, Cai Y, Chen T, Dymond JS,
938 Kang K, et al. 2016. SCRaMbLE generates designed combinatorial stochastic diversity in
939 synthetic chromosomes. *Genome Res* 26: 36–49.

940 Smith AC, Morran LT, Hickman MA. 2022. Host defense mechanisms induce genome
941 instability leading to rapid evolution in an opportunistic fungal pathogen. *Infect Immun* 90:
942 e00328-21.

943 Smith CE, Llorente B, Symington LS. 2007. Template switching during break-induced
944 replication. *Nature* 447: 102–105.

945 Spielmann M, Lupiáñez DG, Mundlos S. 2018. Structural variation in the 3D genome. *Nat*
946 *Rev Genet* 19: 453–467.

947 Sreenivasan VKA, Yumiceba V, Spielmann M. 2025. Structural variants in the 3D genome as
948 drivers of disease. *Nat Rev Genet* 26: 742–760.

949 Storchová Z, Breneman A, Cande J, Dunn J, Burbank K, O'Toole E, Pellman D. 2006.
950 Genome-wide genetic analysis of polyploidy in yeast. *Nature* 443: 541–547.

951 Sun L, Li H, Yan T, Fang T, Wu H, Cao Y, Lu H, Jiang Y, Yang F. 2023. Aneuploidy mediates
952 rapid adaptation to a subinhibitory amount of fluconazole in *Candida albicans*. *Microbiol*
953 *Spectr* 11: e03016-22.

Downloaded from genome.cshlp.org on November 29, 2026 . Published by Cold Spring Harbor Laboratory Press

954 Sun W, Xiong D, Ouyang J, Xiao X, Jiang Y, Wang Y, Li S, Xie Z, Wang J, Tang Z, et al.
955 2024. Altered chromatin topologies caused by balanced chromosomal translocation lead to
956 central iris hypoplasia. *Nat Commun* 15: 5048.

957 Takagi Y, Akada R, Kumagai H, Yamamoto K, Tamaki H. 2008. Loss of heterozygosity is
958 induced in *Candida albicans* by ultraviolet irradiation. *Appl Microbiol Biotechnol* 77: 1073–
959 1082.

960 Thrash-Bingham C, Gorman JA. 1992. DNA translocations contribute to chromosome length
961 polymorphisms in *Candida albicans*. *Curr Genet* 22: 93–100.

962 Todd RT, Braverman AL, Selmecki A. 2018. Flow cytometry analysis of fungal ploidy. *Curr*
963 *Protoc Microbiol* 50: e58.

964 Todd RT, Forche A, Selmecki A. 2017. Ploidy variation in fungi: polyploidy, aneuploidy, and
965 genome evolution. *Microbiol Spectr* 5: FUNK-0051-2016.

966 Todd RT, Selmecki A. 2020. Expandable and reversible copy number amplification drives
967 rapid adaptation to antifungal drugs. *eLife* 9: e58349.

968 Todd RT, Wikoff TD, Forche A, Selmecki A. 2019. Genome plasticity in *Candida albicans* is
969 driven by long repeat sequences. *eLife* 8: e45954.

970 Yadav V, Sun S, Coelho MA, Heitman J. 2020. Centromere scission drives chromosome
971 shuffling and reproductive isolation. *Proc Natl Acad Sci* 117: 7917–7928.

972 Yahya G, Menges P, Amponsah PS, Ngandiri DA, Schulz D, Wallek A, Kulak N, Mann M,
973 Cramer P, Savage V, et al. 2022. Sublinear scaling of the cellular proteome with ploidy. *Nat*
974 *Commun* 13: 6182.

975 Yang F, Kravets A, Bethlendy G, Welle S, Rustchenko E. 2013. Chromosome 5 monosomy
976 of *Candida albicans* controls susceptibility to various toxic agents, including major
977 antifungals. *Antimicrob Agents Chemother* 57: 5026–5036.

Downloaded from genome.cshlp.org on November 29, 2026 . Published by Cold Spring Harbor Laboratory Press

978 Yang F, Scopel EFC, Li H, Sun LL, Kawar N, Cao YB, Jiang YY, Berman J. 2023. Antifungal
979 tolerance and resistance emerge at distinct drug concentrations and rely upon different
980 aneuploid chromosomes. *mBio* 14: e00227-23.

981 Yang F, Teoh F, Tan ASM, Cao Y, Pavelka N, Berman J. 2019. Aneuploidy enables cross-
982 adaptation to unrelated drugs. *Mol Biol Evol* 36: 1768–1782.

983 Yang F, Todd RT, Selmecki A, Jiang Y, Cao Y, Berman J. 2021. The fitness costs and
984 benefits of trisomy of each *Candida albicans* chromosome. *Genetics* 218: iyab056.

985 Yang F, Zhang L, Wakabayashi H, Myers J, Jiang Y, Cao Y, Jimenez-Ortigosa C, Perlin DS,
986 Rustchenko E. 2017. Tolerance to caspofungin in *Candida albicans* is associated with at
987 least three distinctive mechanisms that govern expression of *FKS* genes and cell wall
988 remodeling. *Antimicrob Agents Chemother* 61: e00071-17.

989

Downloaded from genome.cshlp.org on November 29, 2026 . Published by Cold Spring Harbor Laboratory Press

FIGURE LEGENDS

Figure 1. Generation of genomic rearrangements with RED-Cas9 system.

(A) Schematic of the RED-Cas9 system. Single-guide RNAs direct Cas9 to form double-strand breaks (DSBs) at repeat loci (red), resulting in genomic rearrangements.

(B) Distribution of RED-Cas9 target repeats (MRS elements and TREs). Schematic illustrates the karyotype of SC5314, including the following features: telomeres (TEL); MRS elements (comprising RB2, RPS, and HOK); centromeres (CEN); TREs and *TLO* genes.

(C) CHEF electrophoresis gels showing the karyotypes of the WT parental strain and of strains generated by RED-Cas9 targeting of MRS or TRE loci in clinical isolate SC5314.

(D) CHEF electrophoresis gels showing the karyotypes of the WT parental strain and of MRS-targeted RED-Cas9 strains in the WO-1 clinical isolate background. WO-1 chromosomes labeled as rearrangements relative to SC5314 (Selmecki et al. 2010).

(E) CHEF electrophoresis gel of NG strains transformed with the CRISPR-Cas9 cassette without a sgRNA.

Figure 2. ONT sequencing reveals that the RED-Cas9 system generates diverse classes of on-target structural variants.

Karyotype plots based on ONT analysis, with annotated features as in Fig. 1B. Supporting plots provided for loss of heterozygosity (LOH) and copy-number variants (CNVs).

(A) Balanced rearrangements. Chimeric chromosomes arise from balanced rearrangements at MRS loci in MRS-g1 (involving Chr1, Chr4, Chr5, and Chr7) and at *TLO*/TRE loci in TRE-g1 (Chr1;Chr4) and TRE-g5 (Chr1;Chr2 and Chr1;Chr3), each with truncation of Chr1 at *TLO34*.

(B) Loss of heterozygosity. Repeat-associated genomic rearrangements in MRS-g3 (Chr5;ChrR; homozygous), TRE-g3 (Chr1;Chr4), and TRE-g4 (Chr1;Chr3 and Chr1;Chr7) are accompanied by repeat-associated LOH in MRS-g3 (Chr5 distal to MRS-5, and ChrR upstream of RB2) and TRE-g4 (Chr1, upstream of TLO34), as well as whole-chromosome LOH in TRE-g3 (Chr6).

Downloaded from genome.cshlp.org on November 29, 2026 . Published by Cold Spring Harbor Laboratory Press

(C) Heatmap of allelic frequency against the A22 reference genome for strains MRS-g3, TRE-g3, and TRE-g4. The eight *C. albicans* chromosomes are shown, along with haplotype A (green), haplotype B (magenta), and AB (gray).

(D) Segmental copy-number variation in TRE-g6, which harbors TRE-driven interchromosomal rearrangements (Chr1;Chr2 and Chr3;Chr1), complete LOH of Chr6, and three copies of the right arm of Chr1 (truncated at *TLO34*).

(E) Plot shows allele frequency and estimated copy-number of TRE-g6 against the MRS-corrected A22 haplotype A in 10 kb windows.

Figure 3. RED-Cas9 edited strains exhibit whole-chromosome copy-number variation and ploidy change.

(A) Flow cytometry of propidium-iodide-stained cells of WT SC5314 and MRS-g2. SC5314 displays a major 2N peak and secondary 4N peak. MRS-g2 shows loss of the diploid peak, a major peak at 4N and the emergence of a peak at higher DNA content consistent with a shift toward tetraploidy.

(B) Confocal microscopy of ConA–Alexa Fluor 594 and Hoechst-stained WT and MRS-g2 cells following 3 h growth in YPD at 30 °C or 37 °C. ≥1,200 cells were quantified per strain and temperature. Points show biological replicates (n = 3); counts were analyzed at image level by linear mixed-effects models (strain fixed, biological replicate random) with Holm-adjusted contrasts. ****P*adj < 0.001.

(C-D) Karyotype plots based on ONT analysis, with annotated features as in Fig. 1B.

(C) Whole-genome copy-number variation shown for MRS-g2, with tetraploidy and three copies of Chr4 and ChrR, in addition to loss of heterozygosity (LOH) of Chr2 and segmental amplification at RB2 on Chr3B. Schematics illustrate the karyotype of each strain.

(D) Chromosome copy-number variation in TRE-g2 (trisomy Chr5), accompanied by Chr1;Chr3 and Chr4;Chr1 translocations in addition to Chr1 LOH upstream of *TLO34.* Chromosome copy-number in TRE-g7 (Chr4, ChrR trisomies) in addition to Chr1;Chr3 and Chr5;Chr1 translocations.

Downloaded from genome.cshlp.org on November 29, 2026 . Published by Cold Spring Harbor Laboratory Press

(E) Plot shows allele frequency and estimated copy-number of MRS-g2, TRE-g2, TRE-g7 against the MRS-corrected A22 haplotype A in 10 kb windows. MRS-g2 is plotted against a diploid baseline.

(F) Laboratory evolution of balanced MRS-g1 and TRE-g5 strains. Top: Schematics of the evolution: nine colonies per strain were passaged every 48 hours for 10 passages; Bottom Left: CHEF electrophoresis of the parental WT strain and MRS-g1 evolved colonies (a-i); Bottom Right: CHEF electrophoresis of the parental WT strain and TRE-g5 evolved colonies (a-i).

Figure 4. Balanced rearrangements have little effect on gene expression, unlike copy-number variation and loss of heterozygosity.

Differential expression compared to SC5314 on n ≥ 3 biological replicates per strain, apeglm-shrunken $\log_2$ fold changes and Benjamini–Hochberg–adjusted *P*-values. Significance thresholds were $|\log_2 FC| \geq 0.5$ and *P*adj < 0.05. For visualization, fold-change values were capped at ±5 and $-\log_{10}$(*P*adj) at 30.

(A) Volcano plots of differential gene expression in balanced RED-Cas9 strains (MRS-g1, TRE-g1, and TRE-g5).

(B) Shrunken $\log_2$ fold changes of genes whose midpoint lies within 10 kb of rearrangement breakpoints. Breakpoint genomic positions are indicated above and gene names below; asterisks mark significant differential expression.

(C) Volcano plots of differential gene expression in loss of heterozygosity RED-Cas9 strains (MRS-g3, TRE-g3, and TRE-g4) relative to SC5314.

(D) Volcano plots of differential gene expression in copy-number variant RED-Cas9 strains (MRS-g2 and TRE-g7) relative to SC5314.

(E) Mean number of significant DEGs per genome type ± SEM, with individual strains overlaid. * Tukey HSD on $\log_{10}$ DEG counts, *P*adj < 0.05.

Downloaded from genome.cshlp.org on November 29, 2026 . Published by Cold Spring Harbor Laboratory Press

Figure 5. Balanced rearrangements are phenotypically silent, whereas copy-number variation drives phenotypic change in RED-Cas9 strains.

Phenotypic characterization: balanced (MRS-g1, TRE-g1, TRE-g5), LOH (MRS-g3, TRE-g3, TRE-g4) and CNV (MRS-g2, TRE-g2, TRE-g6, TRE-g7) strains. (A) Heatmap of stress-specific fitness (area under the growth curve, AUC) of RED-Cas9 strains across temperature (30 °C, 37 °C, 39 °C), pH (4.5, 2.0), low glucose (0.2%), osmotic (1 M NaCl), oxidative (5 mM H_2O_2), cell wall (10 mM caffeine) stress, and fluconazole (Flc; 2 µg/mL). 30 °C column shows basal fitness relative to SC5314. Other columns are double normalized to 30 °C (DMSO for Flc) and SC5314 (log_2 scale; 0 = equal fitness; n = 3 biological replicates); * mark significant differences from SC5314 (linear mixed-effects models on log_2 AUC with Holm-adjusted contrasts; *P*adj < 0.05 and ≥1.5-fold).

(B) Heatmap showing relative fitness in fungicidal drugs, amphotericin B (AmB) and caspofungin (Cas) derived from microplate dilution assays. Growth was normalized first to the corresponding drug-free YPD control and then to SC5314 growth at the SC5314 MIC_{50} concentration for each drug and time point; * mark significant differences from SC5314 (linear mixed-effects models on log_2 OD with Holm-adjusted contrasts; *P*adj < 0.05 and ≥1.5-fold).

(C) Microplate dilution assay for TRE-g7. Relative fitness normalized to YPD. Estimated MIC_{50} (50% inhibition threshold) and MIC_{90} (90% inhibition threshold) were <2 µg/mL for SC5314 and all RED-Cas9 strains apart from TRE-g7, which increased to 4 and >256 µg/mL, respectively.

(D) Colony filamentation assay. Left: representative RED-Cas9 colony morphology on YPD, spider and RPMI media for parental WT and RED-Cas9 edited strains. Right: Quantification of filamentous, intermediate, or non-filamentous morphologies. Strains are grouped into genome types. CNV strains produced significantly fewer filamentous colonies than WT on YPD, Spider and RPMI (linear mixed-effects models with strain and biological replicate as random effects, Holm-adjusted contrasts; *P*adj= 0.00074, 0.0014 and <0.0001, respectively). Data show mean ± SEM across biological replicates.

Downloaded from genome.cshlp.org on November 29, 2026 . Published by Cold Spring Harbor Laboratory Press

(E) Kaplan–Meier survival in the *Galleria mellonella* model, grouped by genome type. Curves and shaded 95% intervals are unadjusted Kaplan–Meier estimates. Survival differences per group were assessed using a mixed-effects Cox model (coxme), hazard ratios are against SC5314, with BH-adjusted *P*-values. Only the CNV group exhibits significantly reduced virulence (HR = 0.60, *P*adj = 5.6×10^{-4}), driven largely by MRS-g2 (HR = 0.21; Supplemental_Fig_S15). The CNV group effect was not retained when strain was modelled as a random effect (*P* = 0.24) unless restricted to the three whole-chromosome aneuploids (HR = 0.48, *P* = 0.049). ****P*adj < 0.001.

(F) Fluconazole MICs of MRS-g1(Cas9) and its evolved derivative. Plating CFUs on YPD + 8 µg/mL fluconazole resulted in the acquisition of resistance in MRS-g1(Cas9)R which was maintained following passaging in YPD (MIC_{50}: 32 µg/mL; MIC_{90}: 256 µg/mL, from parental MRS-g1(Cas9) MIC_{50}: < 2 µg/mL; MIC_{90}: < 2 µg/mL).

(G) Fluconazole-evolved strain MRS-g1(Cas9)R shows a segmental duplication of the left arm of ChrR with a breakpoint at MRS-R. Allele frequency and estimated copy-number against the MRS-corrected A22 haplotype A in 10 kb windows. Copy-number was estimated from ONT read depth normalized to the trimmed genome-wide mean depth of the SC5314 ONT control. The eight *C. albicans* chromosomes are shown.

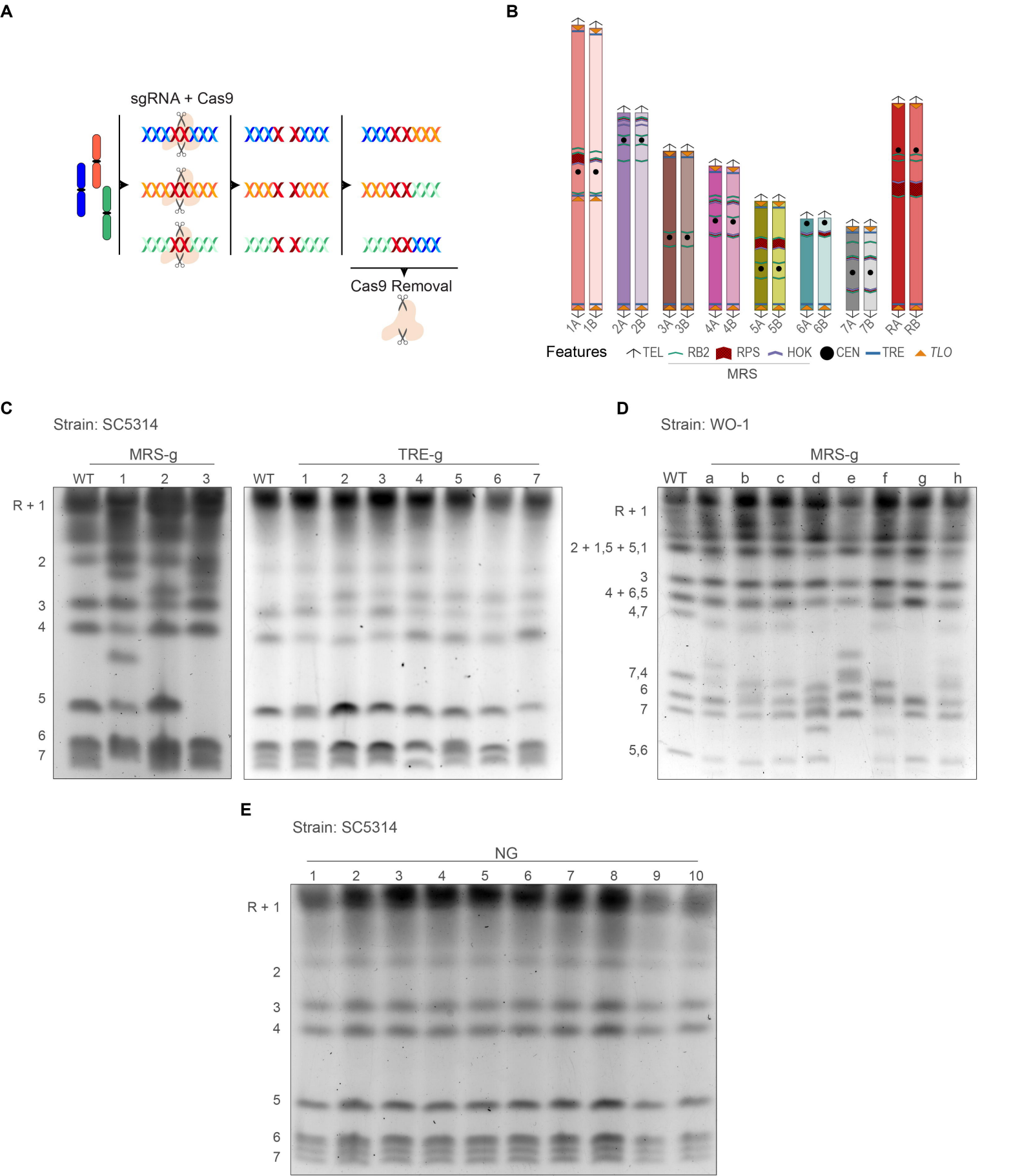
A
sgRNA + Cas9
Cas9 Removal
B
1A
1B
2A
2B
3A
3B
4A
4B
5A
5B
6A
6B
7A
7B
RA
RB
Features
TEL
RB2
RPS
HOK
CEN
TRE
TLO
MRS
C
Strain: SC5314
MRS-g
WT
1
2
3
TRE-g
WT
1
2
3
4
5
6
7
R + 1
2
3
4
5
6
7
D
Strain: WO-1
MRS-g
WT
a
b
c
d
e
f
g
h
R + 1
2 + 1,5 + 5,1
3
4 + 6,5
4,7
7,4
6
7
5,6
E
Strain: SC5314
NG
1
2
3
4
5
6
7
8
9
10
R + 1
2
3
4
5
6
7

Downloaded from genome.cshlp.org on November 29, 2026 . Published by Cold Spring Harbor Laboratory Press

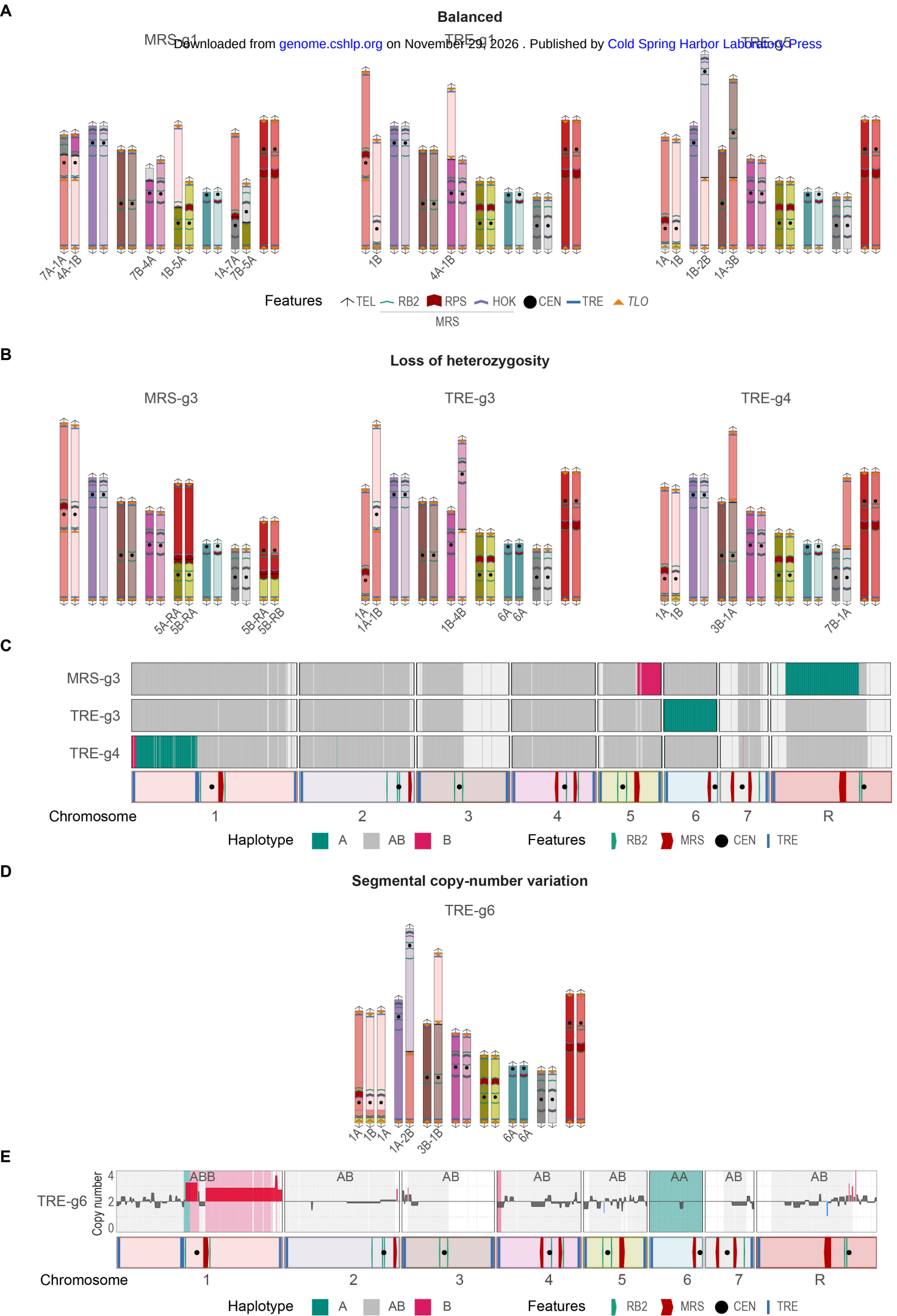

Downloaded from genome.cshlp.org by Cold Spring Harbor Laboratory Press

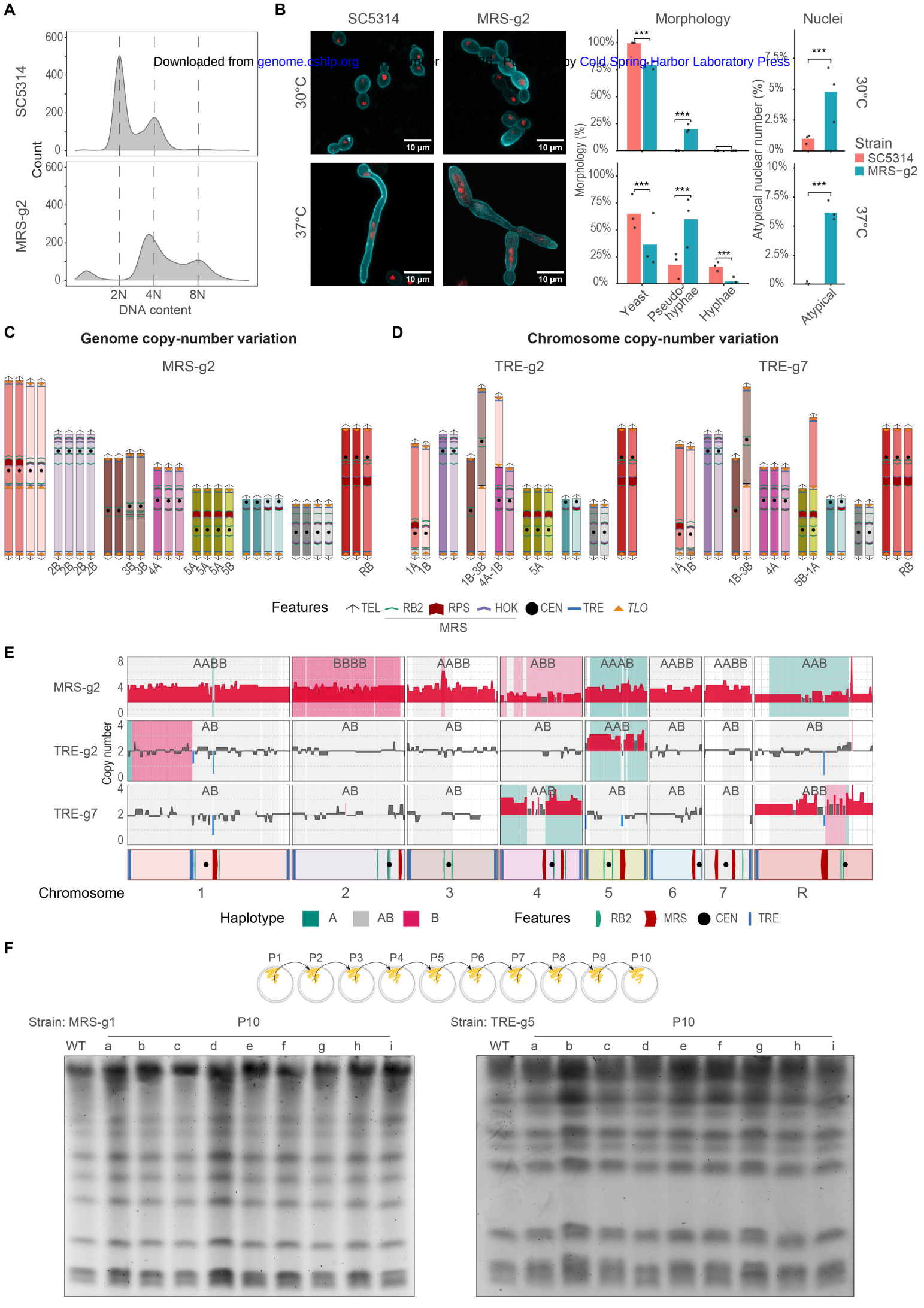

Downloaded from genome.cshlp.org on November 29, 2026 . Published by Cold Spring Harbor Laboratory Press

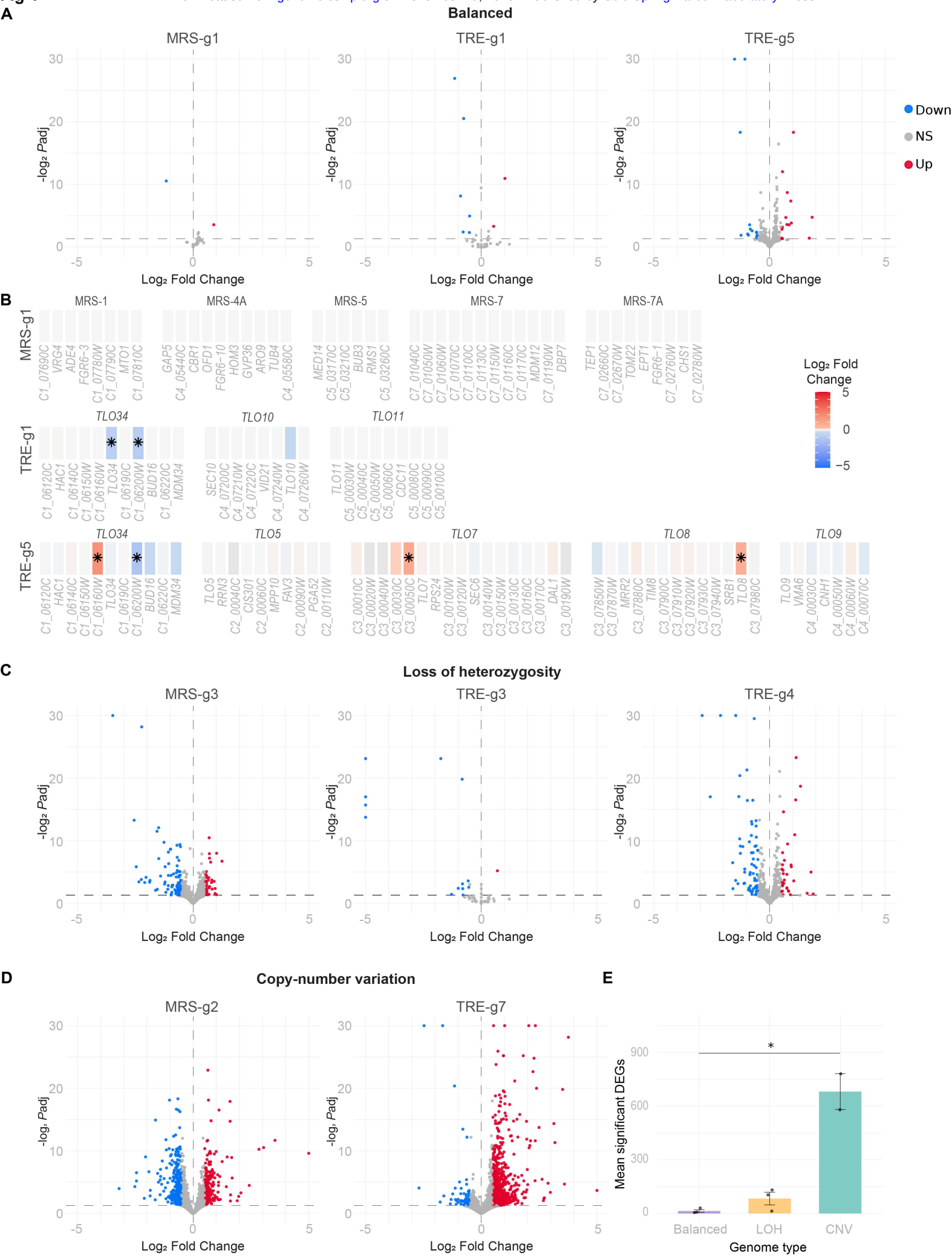

Downloaded from genome.cshlp.org on November 29, 2026 . Published by Cold Spring Harbor Laboratory Press

